PERGAMON

Progress in Crystal Growth and Characterization of Materials (1999)73–132

Progress in Crystal Growth and Characterization of Materials

Bridgman growth: modelling and experiments

J.P. Garandet and T. Alboussière June 3, 1999

Contents

0960-8974/99/$ - see front matter © 1999 Published by Elsevier Science Ltd. All rights reserved.
PII: S0960-8974(99)00010-8

NOMENCLATURE

C	solute composition (mass fraction)
D	solute diffusion coefficient $(m^2.s^{-1})$
$\mathbf{g}$	gravity $(m.s^{-2})$
H	typical small dimension of the cavity (m)
L	length of the liquid domain (m)
m_L	slope of the liquidus $(K.wt\%^{-1})$
$\mathbf{n}$	unit vector normal to a melt boundary, directed in the fluid
U, V, W	dimensional velocity components on the X, Y and Z axis $(m.s^{-1})$
$\mathbf{V}$	mass average velocity of the Navier Stokes equation $(m.s^{-1})$
V_{eff}	effective transport velocity $(m.s^{-1})$
V_I	interface velocity $(m.s^{-1})$
X, Y, Z	dimensional space coordinates (m)
∇	Nabla operator
$\mathbf{B}$	magnetic field (T)
$\mathbf{J}$	electric current density field $(A.m^{-2})$
$\mathbf{M}$	magnetic moment density $(A.m^{-1})$
T	temperature field (K)
G or G_D	temperature gradient $(K.m^{-1})$
G_C	solute composition gradient $(wt\%.m^{-1})$

Greek

α	heat diffusivity $(m^2.s^{-1})$
β	thermal expansion coefficient $(K^{-1}$
	or solute expansion coefficient $wt\%^{-1})$
δ	solute boundary layer thickness (m)
δ_D	solute boundary layer thickness in the diffusive case $(\delta_D = D/V_I, m)$
δ_{SF}	stagnant film thickness in the BPS model (m)
ν	kinematic velocity of the melt $(m^2.s^{-1})$
ρ	mass density $(kg.m^{-3})$
ω	pulsation of the perturbation (s^{-1})
σ	electrical conductivity $(\Omega^{-1}.m^{-1})$
Ψ	streamfunction $(m^2.s^{-1})$
γ	surface tension coefficient $(J.m^{-2}.K^{-1})$
χ_m	magnetic susceptibility [1mm]

Subscripts

L	liquid phase
S	solid phase
I	interface

Superscripts

0	reference "steady" state
1	fluctuation

Dimensionless numbers

$Ha = \sqrt{\frac{\sigma}{\rho\nu}}BH$	Hartmann number
$Gr = \frac{\beta g G H^4}{\nu^2}$	Grashof number
$Sc = \frac{\nu}{D}$	Schmidt number
$Pr = \frac{\nu}{\alpha}$	Prandtl number
$Ra = GrPr$	Rayleigh number
$Pe = \frac{V_L H}{D}$	solute Péclet number
ϵ	aspect ratio $(\frac{H}{L})$
j	complex number $j^2 = -1$
k	solute partition coefficient in a dilute binary alloy
u, v, w	non dimensional velocity components
x, y, z	non dimensional coordinates
Δ	convecto diffusive parameter $(0 \leq \Delta \leq 1)$
Δ_{SF}	parameter to be used in the stagnant film model
Ω	non-dimensional pulsation, $\Omega = \omega\delta^2/D$
ψ	non-dimensional streamfunction

1 Introduction

In the Bridgman growth technique, a crucible containing a polycrystalline feed is introduced into a gradient furnace. After the melting of the feed, growth is initiated by an imposed displacement of the isotherms. This can be done by moving the crucible or the thermal unit, and also by programming the cooling of the various parts of the furnace, everything remaining static. This latter technique, referred to as "Gradient Freeze", allows a suppression of the mechanical vibrations, but induces a coupling between the temperature field and the growth velocity. With respect to gravity, the apparatus can be either aligned (vertical configuration) or perpendicular (horizontal configuration).

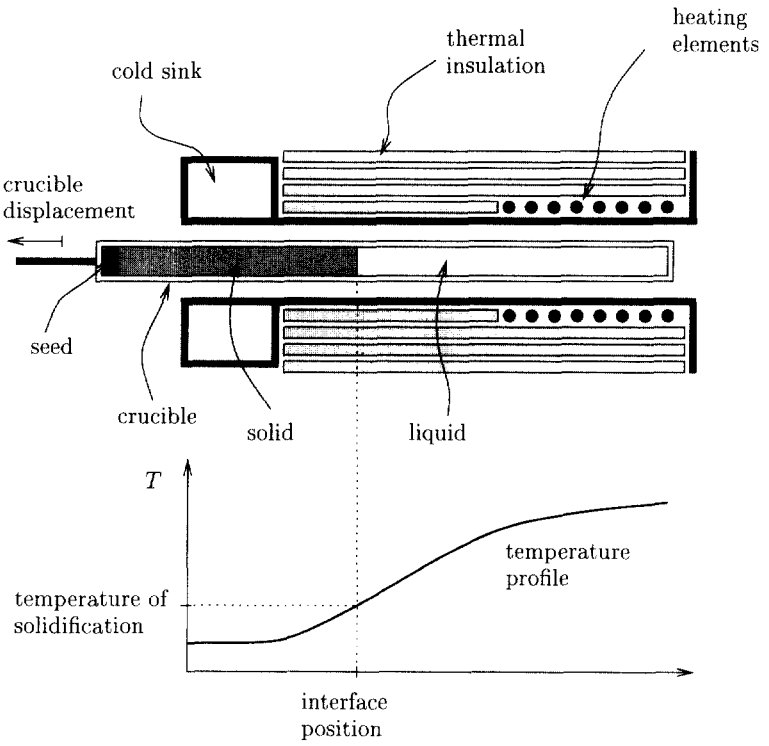

Figure 1: A sketch of the Bridgman configuration

A single crystal seed is often inserted in the crucible to impose the crystallographic orientation of the solidified material, but unseeded Bridgman growth is also commonly used. The Bridgman technique has been used on a variety of materials, e.g. III–V and II-VI semiconductor compounds [1, 2, 3, 4], and oxides, including superconductors [5, 6]. Among all growth configurations, it allows the best control of the experimental conditions, since the thermal gradient can be to a large extent tailored to fit the user's needs. This can lead for instance to a

reduction of the thermomechanic stresses, and thus to a better structural quality of the grown crystals with respect to other solidification techniques. Nevertheless, its industrial use remains limited, which may be due to the fact that available products are often of sufficient quality to meet the user's requirements.

Besides, one should not forget about the specific difficulties of the Bridgman technique, the main one being the direct contact between crucible and growing material. Such a contact can induce parasitic grain generation and adhesion stresses. When available, encapsulants are a promising way to bypass the problem [7]. The crucible is also a source of contamination in the grown crystals. In the horizontal Bridgman configuration, the presence of an uncovered fluid surface allows to control the composition of volatile species using a source material at a controlled temperature, but such a free surface can also lead to Marangoni driven flow instabilities.

Magnetic fields are known to modify the heat and mass transport in the melt, due to the Lorentz force term in the Navier-Stokes equations that govern fluid flow. As for the other growth techniques, the damping action of steady fields was first investigated, dating back to the pioneering work of Utech and Flemings [8]. It was first realized that relatively modest fields were very efficient in damping undesirable convective flow oscillations and the induced temperature and composition fluctuations. For a detailed understanding of the physical mechanisms involved in this stabilization effect, the interested reader is referred to Prof Moreau's contribution in the present book, but one can mention at this point that Joule dissipation in the melt is a key factor.

Later on, research focused on the potential of steady magnetic fields in the tesla range to act on solute incorporation in the crystal at the macroscopic (*i.e.* sample) scale. It was hoped that a significant improvement in terms of both axial and radial segregation could be achieved. More specifically, the convection damping effect of the magnetic field was expected to provide diffusion controlled solute transport conditions, similar to those obtained in microgravity conditions. Some interesting results were thus obtained in terms of solute segregation [9, 10], but the fields required to reach truly diffusion controlled conditions seem to be very high.

More recently, rotating magnetic fields appeared as a promising way to act on melt flow [11, 12]. As opposed to the case of steady fields, the experimental objective is now to increase the convection level through the driving action of the Lorentz force and to obtain an enhanced, but steady, fluid flow. The convection velocity is primarily directed along the azimuthal direction, but a secondary meridional flow is also expected to take place. Besides, even in low Prandtl numbers materials such as liquid metals and semiconductors, a significant effect of the flow on heat transport can be expected. Such an effect can in principle obviate the need for sample and/or crucible rotation used in other solidification techniques.

Nevertheless, most of the research carried out on the use of magnetic fields in the Bridgman growth configuration was directed on the problem of solute repartition in alloy crystals. We thus think it worthwhile to spend some time in section 2 to outline the basic mechanisms of segregation, with a special emphasis on the solutal boundary layer concept. Then, in section 3, a review of the stabilizing effect of a steady field on hydrodynamic fluctuations will be presented. Sections 4 and 5 are respectively dedicated to the problems of magnetic damping

of steady flows and to rotating field mixing. Finally, in section 6, miscellaneous questions such as thermoelectricity or magnetic forces will be addressed. In all cases, our review will include modelling and experimental results.

Since the theoretical frame of our topic is covered in Prof Moreau's contribution in the present book, we shall not come back to the formulation of magnetohydrodynamics, but rather focus on its implications in Bridgman growth. We shall thus start with standard equations, and refer the interested reader to Prof Moreau for a discussion of the underlying hypotheses. However, one should be aware that a critical examination of modelling assumptions is always necessary. For instance, as shown by Walker and Williams [13] in their study of the Czochralski silicon growth, the widely used hypothesis that a solid semiconductor is electrically insulating with respect to its metallic melt can lead to erroneous conclusions.

2 Background on solute segregation

Our purpose in this section is to briefly recall the relevant transport equations and to outline the mechanisms governing the physics of solute segregation in alloy crystals. We shall lay a special emphasis on the role of convection in the problem, and stress the need to quantify and act on the fluid velocity, *e.g.* through the application of magnetic fields, and more specially in the Bridgman configuration. The interested reader is referred to standard reference works for more general information on the topic of solute segregation [14, 15, 16, 17, 18].

2.1 Statement of the problem

In view of the low solidification rates used for crystal growth, we shall consider that thermodynamic conditions prevail at the interface. The phase diagram of the alloy system thus yields a local relation between the compositions of the solid and liquid phases, and all segregation phenomena stem from the difference between these compositions. For the sake of simplicity, let us consider a binary alloy consisting of a solvant and a single solute, and assume the mass densities of the fluid and the solid to be equal. In mathematical terms, the condition that the excess (resp. missing) solute on the liquid side of the front has to diffuse away from (resp. towards) the interface can be written as :

$$D_S \left(\frac{\partial C_S}{\partial n}\right)_I - D_L \left(\frac{\partial C_L}{\partial n}\right)_I = (C_{LI} - C_{SI})\mathbf{V}_I.\mathbf{n}, \tag{1}$$

where C_{LI} and D_L (resp. C_{SI} and D_S) stand for the solute composition at the interface and diffusion coefficient in liquid (resp. solid) phase, $\mathbf{V}_I$ the solidification velocity imposed by the furnace and $\mathbf{n}$ the normal to the growth interface pointing in the fluid. As for solute repartition, a classical mass conservation equation can be written in both phases :

$$\rho\frac{\partial C}{\partial t} + \nabla\mathbf{J}^M = 0. \tag{2}$$

In the fluid, the total mass flux $\mathbf{J}^M$ can be taken as the sum of a diffusive and a convective term :

$$\mathbf{J}_L^M = \rho(-D_L\nabla C + \mathbf{V}C), \tag{3}$$

with **V** standing for the fluid flow velocity as given by the Navier-Stokes equation if the solute composition is given in mass fraction. Other units could in principle be used, and it can indeed be shown that a similar formulation can be written in terms of molar fraction in dilute alloys [18], but for the sake of consistency we shall keep on using mass fractions.

In the solid phase, only diffusive transport is to be considered, but it should be noted that the values of D_S are extremely low (say in the range from 10^{-15} to $10^{-11} m^2.s^{-1}$), meaning that, once incorporated, the solute is essentially frozen in the crystal. In the following, we shall thus omit solid state diffusion from the formulation of the problem, and, unless otherwise specified, restrict ourselves to the study of liquid phase solute transport. This will allow us to drop the subscripts from D_L and C_L.

Since we are in this section mostly interested in a presentation of relevant solute segregation mechanisms, we shall not consider other potential contributions in the expression of the mass flux. Nevertheless, the reader should be convinced that other driving forces, such as thermodiffusion, may have an impact on the solidification process [19, 20]. It should also be mentioned that, in a polyconstituted alloy, a boundary condition and a conservation equation similar to eqs. (1) and (2) could be written for each solute.

As the Navier Stokes equation is thoroughly discussed in the introducing chapter of this handbook, we only need to state it in the form we shall use, namely :

$$\rho\left(\frac{\partial \mathbf{V}}{\partial t} + (\mathbf{V}.\nabla)\mathbf{V}\right) = -\nabla P + \rho\nu\nabla^2\mathbf{V} + \mathbf{F}_{ext}. \tag{4}$$

In our present problem the external force $\mathbf{F}_{ext}$ is the sum of a gravity and a Lorentz term :

$$\mathbf{F}_{ext} = \rho\mathbf{g} + \mathbf{J} \wedge \mathbf{B}. \tag{5}$$

The dependence of the mass density on temperature and composition induces a coupling between the hydrodynamic, thermal and solute fields. For a meaningful use of magnetic fields, the fluids have to be relatively good conductors of electricity, and most of them will also be good heat conductors. In view of the limited natural convection flow velocities, heat transport can often be considered to proceed mostly by diffusion, specially in the vertical Bridgman configuration, and the thermal problem can thus be decoupled from the others. In addition, in dilute alloys, the dependence of mass density on composition can often be neglected, meaning that the Navier Stokes equation can be solved independently from the composition field.

However, these convenient approximations may prove misleading; indeed, we shall see in section 5 that the relatively fast fluid motions driven by rotating magnetic fields contribute significantly to heat transport. In practice, one should always derive a thermal Péclet number, $Pe_T = VH/\alpha, H$ being a typical dimension of the cavity and α the heat diffusivity of the fluid, to check the validity of the assumption. As for the dilute alloy approximation, its range of validity will be discussed in section 2.5.

For the time being, we shall consider the fluid velocity to be a given input in the solute conservation equation, that, in a reference frame moving with the interface, can be written as :

$$\frac{\partial C}{\partial t} + (\mathbf{V}.\nabla)C = D\nabla^2 C + (\mathbf{V}_I.\nabla)C. \tag{6}$$

The idea of using such a reference frame stems from the possibility of reaching steady state mass transport conditions, which is obviously not the case in the laboratory frame due to interface motion. As a further simplifying assumption, the partition coefficient k, defined as $k = C_{SI}/C_{LI}$ will be taken as constant all over the composition range. We shall also consider the solid liquid interface to be planar, with its normal pointing in the Z direction and aligned with the growth velocity. Eq. (1) can thus be re-written as :

$$-D(\partial C/\partial Z)_I = V_I(1-k)C_I. \tag{7}$$

The problem formulation, as stated by eqs. (1) to (7) is now complete, and we can now turn to the study of segregation mechanisms, and more specially to a presentation of the solute boundary layer concept.

2.2 The solute boundary layer concept

The existence of a solute rich (resp. depleted) region ahead of the growth front when the partition coefficient k is smaller (resp. higher) than unity is a fact now well accepted. Numerous results, both from experimental data [21, 22, 23] and from numerical simulations (see *e.g.* [24, 25, 26, 27]) support such an assumption. It is important to be aware that such a boundary layer should not be taken as a stagnant film where mass transport proceeds mainly by diffusion. The confusion that can be found in the literature can be traced back to the followers of the pioneering work of Burton, Prim and Schlichter [28], where the authors set up to solve the solute transport problem in an idealized Czochralski configuration.

In this key paper [28] the existence of a solutal boundary layer was first stressed, and a method proposed to estimate its thickness. The authors then proceeded to show that similar results in terms of interface concentration could be obtained assuming a stagnant film of thickness δ_{SF}, but, to quote their own words "the somewhat arbitrary quantity δ_{SF} may be characterized by defining it so that it yields the same dependence of the composition upon the growth parameters that is given by the exact solution." In other words, they used the stagnant film model for mere mathematical convenience, but their insight was lost to many of their followers.

In any case, due to the existence of a boundary layer ahead of the growth front, the composition variations in the melt will take place over a well defined length scale. Following Wagner and Wilson [29, 30], and denoting C_∞ the concentration in the bulk fluid, *i.e.* far away from the interface, one can define this length scale δ in mathematical terms as :

$$\delta = -\frac{[C_I - C_\infty]}{\left(\frac{\partial C}{\partial Z}\right)_I}. \tag{8}$$

It is thus tempting to use a scaling analysis technique to better understand the influence of the various parameters of the problem, and specially of the convective field. We shall here only outline the procedure to be followed for differential equations, the interested reader being referred to other works for more details on the technique and its fields of applications [31, 32, 33].

Briefly speaking, one first identifies ranges of variations (scales) for each relevant parameter. Then if a variable C is seen to vary from C_1 to C_2 over a length scale $Z_2 - Z_1$, the derivative dC/dZ is approximated by $(C_2 - C_1)/(Z_2 - Z_1)$. With such a technique, one can thus transform the initial differential equation into a much simpler algebraic equation, that, provided the scales have been selected properly, captures the physics of the problem at a much lower computational cost. The method is simple and powerful, but its predictions should always be matched against existing experimental data or numerical simulations for mutual validation.

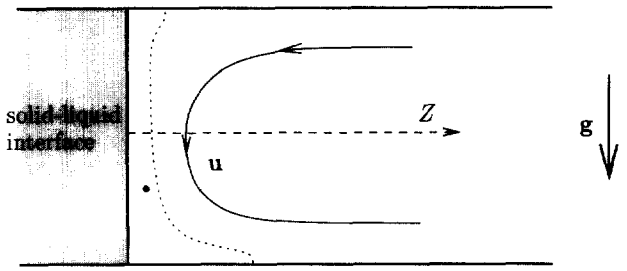

Figure 2: Isoconcentration line near a solid-liquid interface

Let us now turn to our present problem, whose geometry is sketched in fig. 2, of a planar interface moving at a velocity V_I in the Z direction. To apply the scaling analysis technique, eq. (6) must be somewhat transformed. We shall first suppose that the composition variations are mainly in the direction normal to the interface, *i.e.* the Z axis in our case. Such an hypothesis is far from obvious, as the composition field is significantly distorted around the bottom left corner. But to a first approximation, the isoconcentration lines can be considered parallel to the growth interface, at least in the upper part of the cavity (see reference [33]).

Having dropped all radial segregation aspects so far ($\partial C/\partial X = \partial C/\partial Y = 0$), we shall in addition assume a steady state to be reached in the frame moving with the interface ($\partial C/\partial t = 0$). Finally, to make the problem fully one dimensional, let us take the average of the Z component of the fluid velocity W,over the upper half of the melt; denoting $\overline{W}(Z)$ this average convection velocity, eq. (6) becomes :

$$D\frac{d^2C}{dZ^2} + (V_I - \overline{W}(Z))\frac{dC}{dZ} = 0. \tag{9}$$

It should be said that other physically sound choice (e.g. the maximum of W) would yield

similar results in terms of scaling law. From the definition of δ as the relevant length scale for composition variations, C can be assumed to vary from the unknown value C_I at the interface ($Z = 0$) to C_∞ in the bulk fluid over the boundary layer thickness. At the scale δ, one can thus write :

$$\frac{dC}{dZ} \cong -\frac{[C_I - C_\infty]}{\delta}, \quad \frac{d^2C}{dZ^2} \cong \frac{[C_I - C_\infty]}{\delta^2}, \quad \overline{W}(Z) \cong \overline{W}(\delta). \tag{10}$$

After substitution of the above relations in eq. (9) and division by $[C_I - C_\infty]/\delta$, we finally get :

$$\frac{D}{\delta} = V_I - \overline{W}(\delta). \tag{11}$$

When $k \leq 1$, C_I is higher than C_∞, and conversely for $k \geq 1$, but eq. (11) should be valid in both cases. Besides, with our choice of axis orientation, $\overline{W}(\delta)$ is negative. The validity of eq. (11) has been assessed by checking its predictions in a variety of growth configurations, including the semi-analytical solution obtained by Burton, Prim and Schlichter in their model Czochralski problem [34], where a very good agreement was observed.

In Bridgman growth, the predictions of eq. (11) were seen to compare favourably with both numerical [26, 35, 36] and experimental [18] data, but the reader is referred to the original publications for more details on the results. Outside the field of monophased growth, eq. (11) proved to be well adapted to the understanding of transport phenomena in off-eutectic solidification [36].

With all these successes in mind, it appears clearly that what matters is the convection velocity at the boundary layer scale, the details of the hydrodynamic field away from the growth front being of little interest. Procedures allowing to estimate $\overline{W}(\delta)$ in Bridgman configurations in the presence of a steady magnetic field will be presented in section 4.

The stage is now set for some general comments on the physics of the solute transport problem and on segregation phenomena. At the boundary layer edge, eq. (11) shows that a typical diffusive velocity D/δ balances the overall transport velocity $V_{eff} = V_I - \overline{W}(\delta)$ towards the front. Depending on the relative magnitudes of V_I and $\overline{W}(\delta)$, transport will be said to be diffusion controlled ($V_I \gg \overline{W}(\delta)$) or convection controlled ($V_I \ll \overline{W}(\delta)$).

More precisely, one can scale the solutal boundary layer thickness with regard to the reference diffusive transport case first treated by Tiller *et al.* [37]. Indeed, if convective transport can be neglected, an analytical solution can easily be found to the system of eqs. (7) and (8), along with the far field condition :

$$Z \to \infty \qquad C \to C_\infty. \tag{12}$$

In that solution, the composition is seen to decrease exponentially from its value C_∞/k at the interface to its value in the bulk C_∞, over a length scale D/V_I. Applying Wilson's definition, eq. (8), one gets for the reference diffusive case $\delta_D = D/V_I$. The non dimensional number $\Delta = \delta/\delta_D = \delta V_I/D$ can thus be taken as a measure of the convecto-diffusive state of the melt.

Another way to look at the problem is to multiply both sides of eq. (11) by δ/D, and to define a boundary layer solutal Péclet number by $Pe_\delta = -\delta\overline{W}(\delta)/D$, yielding $\Delta + Pe_\delta = 1$. One thus sees that for the Péclet number to be relevant, it must be based on the boundary layer thickness and on the fluid velocity at this scale. Any *a priori* derivation using a typical macroscopic dimension of the cavity and the maximum or average convection velocity in the fluid is prone to be physically meaningless.

The convecto diffusive parameter Δ also appears in the expression of the interface composition, which is of course of key interest for the study of segregation phenomena, since it allows to define an effective partition coefficient (see section 2.3). Indeed, inserting eq. (7) in eq. (8), one easily gets :

$$C_I = \frac{C_\infty}{[1-(1-k)\Delta]}. \tag{13}$$

The interface composition is thus seen to range from C_∞ when $\Delta \to 0$ (total mixing in the melt) to C_∞/k when $\Delta = 1$ (diffusion limited transport). Finally, it is interesting to note that the global features of the concentration field (in terms of interface value and characteristic length scale) can be obtained by solving a simple diffusion equation :

$$D\frac{d^2C}{dZ^2} + V_{eff}\frac{dC}{dZ} = 0, \tag{14}$$

provided that V_{eff} is taken to be equal to $V_I - \overline{W}(\delta)$ (see eq. (9) for comparison). The formulation of eq. (14) is physically more satisfying than the stagnant film model proposed by Burton, Prim and Schlichter, since it avoids the discontinuity in solute flux in $Z = \delta_{SF}$. Besides, we shall see in section 2.4 that the effective velocity model can be adapted to the study of transient segregation problems.

Our purpose here was to outline the importance of the solutal boundary layer concept and the ability of the scaling analysis to capture the physics of transport phenomena. We so far considered only a steady state approach, and we now have to build a link with the applications in terms of segregation in solidified crystals.

2.3 Macrosegregation

2.3.1 Axial segregation

Early models describing solute incorporation along grown crystals considered the limiting cases of diffusion controlled solute transport [37] or total mixing in the melt [38]. One of the key breakthroughs of the famous work of Burton, Prim and Schlichter [28] was to account for general transport conditions by defining an effective partition coefficient k_{eff}, related to the boundary layer thickness, as $k_{eff} = k\, C_I/C_\infty$. Indeed, we get from eq. (13) :

$$k_{eff} = \frac{k}{[1-(1-k)\Delta]}. \tag{15}$$

Assuming this effective partition coefficient to be constant during solidification, and the initial transient necessary for the solute boundary layer buildup to be short enough to ensure that

C_∞ can be identified with the nominal (*i.e.* initial) feed alloy composition C_0, one can write :

$$C_S = k_{eff} C_0 (1 - f_S)^{k_{eff}-1}, \tag{16}$$

with C_S and f_S respectively standing for the crystal composition and the solidified fraction. Eq. 16 is a modified version of the famous Scheil's equation, where the effective partition coefficient k_{eff} has been used for the thermodynamic partition coefficient k. It should be noted that a further hypothesis is necessary in the derivation, namely that the amount of solute in the bulk fluid is large compared to that of the boundary layer.

Eq. 16 can not be valid indefinitely when k_{eff} is smaller than unity, since it predicts the crystal concentration to be infinite in $f_S = 1$. In practice, for the general case of limited solubility in the solid phase, an eutectic or peritectic structure will be formed at a given composition, thus modifying the interface boundary condition. Besides, even for the systems exhibiting total miscibility, the partition coefficient k_{eff} can not be assumed constant when the concentration becomes too high.

Finally, if the ratio of the temperature gradient to the growth velocity is too small, cells or dendrites will be formed over the Mullins-Sekerka morphological stability threshold, see *e.g.* [39, 40, 41]. Even with all these limitations in mind, one should stress the considerable engineering usefulness of eq. (16), which is still the basis for the interpretation of experimental composition profiles in grown crystals.

For the sake of completeness, we should like to give the expression of the effective partition coefficient as initially proposed by Burton, Prim and Schlichter in the frame of their stagnant film model :

$$k_{eff} = k/[k + (1 - k)\exp(-\Delta_{SF})]. \tag{17}$$

In steady state problems, both expressions for k_{eff} can be made to coincide provided that Δ and Δ_{SF} are related by $\Delta = 1 - \exp(-\Delta_{SF})$. Nevertheless, our opinion is that the boundary layer model should preferably used since it precludes the problem of flux discontinuity. Besides, as already stated, we shall see in section 2.4 that it allows to study transient segregation phenomena in a physically sound manner.

Back to our focus on axial segregation, a look on eqs. 15 and 16 will convince the reader that the composition in the grown crystal will be uniform when Δ(or equivalently k_{eff}) is equal to unity, in other words when mass transport proceeds solely by diffusion. Such a result was the driving force for the development of Bridgman microgravity experiments, where it was demonstrated in pioneering works [42, 43, 44] that partitionless solidification could indeed be achieved in space.

Another way to damp bulk natural convection in electrically conducting fluids is to use a steady magnetic field. The numerous results thus obtained in the Bridgman configuration, both vertical and horizontal, will be reviewed in section 4. Briefly speaking, one generally observes an increase in k_{eff} due to the magnetic field. However, one should be aware that the induced

modification of the convection pattern may be detrimental in terms of radial segregation, as a presentation of the relevant mechanisms will clearly show.

2.3.2 Radial segregation

Radial segregation can be defined as the composition variations observed on slices cut perpendicular to the growth direction. Typically, in melt grown semiconductor crystals, the requirements of the device manufacturers are that the wafers should be homogeneous within a few percents. This may not be easily reached in practice, and we need to identify the physical mechanisms leading to radial segregation to assess whether such an objective can be achieved.

The curvature of the solid-liquid interface, hardly avoidable in practice, is an obvious cause of radial segregation. In Bridgman growth, the difference between the thermal conductivities in the solid and liquid phases induces a heat loss to the crucible in the vicinity of the interface, which translates in a deformation of the front. Other factors, such as convective transport or latent heat [45] may also play a role. Technical options to limit the radial temperature gradients have been proposed (see *e.g.* [10, 46, 47, 48]), but in most cases interface curvature is a key factor in radial segregation.

The problem has been solved in some detail by Coriell *et al.* [49, 50] under the assumption of diffusion controlled solute transport. In the low growth velocity range and for small dimensional interface deflections ΔZ, the maximum concentration difference in the solid ΔC_S can be simply expressed as :

$$\frac{\Delta C_S}{C_S} = \frac{V_I}{D}(1-k)\Delta Z, \tag{18}$$

C_S being the local average crystal composition. It should be remembered that the relative radial segregation in the fluid is also given by the right hand side of eq. (18), since both ΔC_S and C_S have to be divided by the partition coefficient k. In the general case of high growth velocities and interface curvature, the problem was solved by numerical simulations [50].

An analytical solution also exists for the asymptotic case of total mixing in the melt [18], where the normalized radial segregation in the low interface curvature limit can be expressed as a function of the solidified fraction :

$$\frac{\Delta C_S}{C_S} = (1-k)(1-f_S)^{-1}\Delta f_S, \tag{19}$$

where Δf_S, the maximum difference in solidified fractions on a slice perpendicular to the growth direction, is directly proportional to the dimensional interface deflection ΔZ.

A common feature to eqs. 18 and 19 is that they both tend linearly to zero with ΔZ. However, partial mixing in the melt can lead to a significant radial segregation even if the interface is perfectly planar. This can be understood qualitatively by considering that moderate convection can significantly distort the isoconcentration lines (see fig. 2). More quantitatively, radial segregation can be said to be governed by variations of the boundary layer thickness along the solid-liquid front. Indeed, eq. (8) can in principle be written at each location on the

interface, thus relating $\delta(X,Y)$ and $C_I(X,Y)$.

The influence of partial mixing on radial segregation for the case of a perfectly planar solidification front has been considered extensively in the horizontal Bridgman configuration using numerical simulations [24, 26], approximate analytical solutions [51] and scaling analyses [52, 53]. As a function of the convection level, the results show that radial segregation starts from zero, increases, passes through a maximum, and then decreases.

A large body papers also focused on the vertical Bridgman configuration, from analytical [54], numerical (see *e.g.* [25, 35, 55, 56, 57]) and experimental [57, 58] standpoints. A typical variation of the radial segregation with the convection level, measured here by the Grashof number Gr, is presented in figure 3, reproduced from ref. [35]. The main difference with the horizontal case is the existence of curvature induced composition variations along the interface at low Gr values, but the existence of a maximum in radial segregation at intermediate convection levels is again observed.

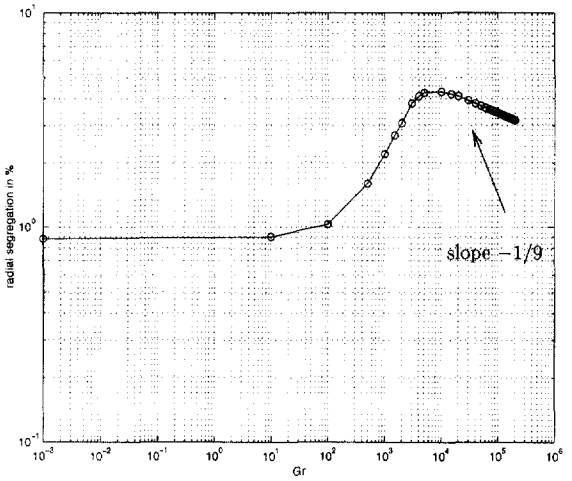

Figure 3: Variation of radial segregation Δc as a function of Gr. After Kaddeche *et al.* [35]

If heat transport in the sample - crucible system is mostly controlled by diffusion, steady magnetic fields can not be expected to act significantly on curvature induced radial segregation. On the other hand, they will modify the convection level solute transport, and may thus increase or decrease the composition variations along the growth front, depending on the growth conditions.

Various scaling laws accounting for the effect of steady magnetic fields in Bridgman configurations will be presented in section 4. It will be seen that both axial and radial segregation need to be considered when selecting experimental conditions. As for rotating magnetic fields,

they will be shown in section 5 to impact on both interface shape and radial segregation [12]. For the time being, we shall now turn to a presentation of the mechanisms of transient solute incorporation to complete this brief overview of segregation phenomena.

2.4 Solute striations (microsegregation)

Unsteady solidification conditions are known to result in transient variations of solute composition, also known as striations or microsegregation, that can be a serious problem for crystal growers. Apparatus related instabilities, such as pulling inhomogeneities or vibrations, lead to fluctuations of the solidification velocity and thus of the interface composition. As for unsteady convection in the melt, it acts directly on the solute field, but also indirectly via the induced variations of the growth rate if the coupling with heat transport is strong enough. Kinetic effects at the atomic level, such as step bunching on faceted interfaces [59, 60], can also result in transient solute incorporation, but will not be considered here since their relation to magnetic fields is far from obvious.

The obtaining of a solution to the problem of solute striations is a formidable task, since it requires the time dependent versions of the heat, momentum and mass conservation equations to be solved simultaneously. In their pioneering work, Hurle *et al.* [61] focused on the effect of a thermal fluctuation on the composition field, and used a stagnant film model to account for convective transport. In their one dimensional perturbation approach, only small deviations with respect to reference "steady state" conditions are considered, and the main variables of the problem (interface velocity, temperature and composition fields) are expanded into Fourier series up to the order one; in terms of concentration for instance, one gets :

$$C(Z,t) = C^0(Z) + C^1(Z)\exp(i\omega t) \tag{20}$$

This approach was later refined by Thévenard *et al.* [62] to lift some minor flaws in the formulation. However, in both cases, due to the physical inconsistency of the stagnant film model, the results may be questionable away from the asymptotic convective transport limit [18]. Fortunately, a similar perturbation approach can be followed in the sounder frame of the boundary layer model [63]; let us thus consider the time dependent version of eq. (14), namely :

$$\frac{\partial C}{\partial t} = D\frac{\partial^2 C}{\partial Z^2} + V_{eff}\frac{\partial C}{\partial Z}. \tag{21}$$

With the help of the above equation, it is possible to define the frequency range of "quasi-steady" perturbations. Indeed, if we denote ω the pulsation of the composition variations, order of magnitude estimates of the $\partial C/\partial t$ and $D\ \partial^2 C/\partial Z^2$ terms are as follows :

$$\frac{\partial C}{\partial t} \cong [C_I - C_\infty]\omega \qquad D\partial^2 C/\partial Z^2 \cong D[C_I - C_\infty]/\delta^2, \tag{22}$$

assuming again that δ is the length scale of the spatial composition variations (see section 2.2). The condition defining "quasi-steady" perturbations ($\partial C/\partial t \ll D\ \partial^2 C/\partial Z^2$) is thus given as :

$$\Omega = \omega\frac{\delta^2}{D} \ll 1. \tag{23}$$

Quite generally, eq. (21) can be solved using Fourier expansion series for both the composition eq. (20) and the effective velocity, with a forcing term V^1_{eff} included :

$$V_{eff} = V^0_{eff} + V^1_{eff} \exp(j\omega t). \tag{24}$$

V^1_{eff} can be related either to a growth ($V^1_{eff} = V^1_I$) or a convective ($V^1_{eff} = V^1_C(Z)$) velocity fluctuation. In the first case, the interface boundary condition eq. (7) should be written using the instantaneous growth rate. As for the second case, a further simplifying assumption is to estimate the relevant convective fluctuation at the boundary layer scale, $V^1_{eff} = V^1_C(\delta)$. Besides, we shall only consider low amplitude fluctuations, such that the second order term $V^1_{eff}C^1$ can be neglected. In such a linear approach, the relation between the effective velocity and composition fluctuations can be adequately characterized by transfer functions, as commonly used by electrical engineers in signal processing.

Even with these assumptions, the algebra involved is fairly tedious, and the interested reader is referred to the original publications [63, 64, 65] for details on the derivation. We shall here only present the results in condensed form and outline the main features of the solutions. For the case of unsteady interface velocity variations, sufficiently far away from the diffusion transport limit, the relation between normalized composition fluctuations and interface velocity fluctuations can be expressed as :

$$C^1_I/C^0_I = [G_S/(1 + j\Omega/\Omega_C)]^{1/2} V^1_I/V^0_I, \tag{25}$$

G_S and Ω_C being respectively the static gain and the cutoff pulsation of this order 1/2 linear filter and j the complex number such that $j^2 = -1$. Numerically, G_S and Ω_C are given as :

$$G_S = (1-k)\Delta(1-\Delta)/[(1-(1-k)\Delta] \tag{26}$$

$$\Omega_C = [(1-(1-k)\Delta)/(1-\Delta)]^2. \tag{27}$$

The above relations demonstrate the ability of the convectodiffusive parameter Δ to capture the physics of segregation phenomena in both steady and transient conditions. When $\Delta \to 1$ (diffusion controlled transport), the order 1/2 linear filter representation is not appropriate, and it is necessary to refer the general form of the solution [63]. Similarly, in the case of unsteady convective fluctuations, the relation between normalized composition fluctuations and convective velocity fluctuations can be expressed as :

$$C^1_I/C^0_I = [G_S/(1 + j\Omega/\Omega_C)] V^1_C(\delta)/V^0_I. \tag{28}$$

G_S and Ω_C are now the static gain and the cutoff pulsation of this first order linear filter, given as :

$$G_S = (1-k)\Delta^2/[(1-(1-k)\Delta] \tag{29}$$

$$\Omega_C = 1-(1-k)\Delta \tag{30}$$

Eqs. (25) to (30) were seen to compare favourably with available numerical [64, 66] and experimental [63, 67] data. From the structure of these equations, it is clear that over a given threshold Ω_C, the perturbations will be filtered out. Conversely, low pulsation fluctuations are

the most harmful in terms of solute segregation.

It should be noted that for both unsteady growth rate and convection mechanisms, Ω_C is often of order of magnitude unity; in dimensional terms, this means that the cutoff pulsation will not exceed 1 Hz, and may be sometimes significantly smaller [64]. Finally, it should be noted that convection controlled transport ($\Delta \rightarrow 0$) results in low levels of segregation, which can be understood in qualitative terms since the melt is then almost homogeneous.

In connection with the results on the effect of steady fields on unsteady convection that will be presented in section 3, it should be again stated that what matters is the amplitude of the hydrodynamic fluctuation at the solute boundary layer scale. However, before turning to a detailed presentation of the results showing the influence of magnetic fields in the Bridgman configuration, we think it worthwhile to discuss briefly the widely used "dilute alloy" approximation.

2.5 The dilute alloy approximation

In many cases of semiconductor growth from the melt, only very small amount of dopants (say in the range of 10 to 100 parts per million) are needed to confer the desired properties to the base material. As for mechanical hardening of the matrix by means of foreign atoms, such as widely used in the Czochralski configuration, the relevant concentrations are significantly higher, but remain limited to the order of some percents at the most. On the other hand, the growth of mixed crystals with adjustable lattice parameters for epitaxy often requires composition variations covering a large portion of the phase diagram. It may thus be interesting to see under what circumstances, and with respect to what kind of problems an alloy can be considered "dilute."

This can first be discussed from a thermodynamic standpoint. Indeed, if the amount of solute becomes too high, the assumptions of constant partition coefficient and liquidus slope can not hold all over the composition range, and one should use the phase diagram of the system to obtain local relations. Other thermophysical parameters, such as diffusion coefficient or kinematic viscosity, may also be thought to depend on concentration; however, even for the most studied materials, some values may not be fully reliable. One should thus be cautious about the validity of the formulations that claim to account for the composition dependence of thermophysical properties.

More interesting for our present purposes of growth under magnetic fields, one may wonder about the hydrodynamic limit of the dilute alloy approximation. Indeed, if solutal convection can be neglected, the transport problem becomes much simpler since the Navier-Stokes and the solute conservation equations can be decoupled. In the horizontal Bridgman configuration of ref. [10], an order of magnitude analysis was used to estimate the ratio between the solutally and thermally driven natural convection flow velocities. At the boundary layer scale, the result can be written as :

$$V_C(\delta)/V_T(\delta) = (\beta_C G_C/\beta_T G_T)(\delta/H)^2, \tag{31}$$

$\beta_T, \beta_C, G_T, G_C$ and H respectively representing the thermal and solutal expansion coefficients, the temperature gradient imposed by the growth furnace, the composition gradient at the interface given by eq. (7) and a typical dimension of the cavity. In many practical cases, (δ/H) is significantly smaller than unity, which means that the dilute alloy approximation may be expected to hold even if the ratio $\beta_C G_C/\beta_T G_T$ is fairly large.

In vertical Bridgman configurations, other forms of coupling between the concentration and hydrodynamic fields can exist. For instance, if the composition gradient ahead of the growth front makes the boundary layer lighter than the bulk liquid, solutal type Rayleigh Bénard convection may take place. An instability threshold can be estimated using the concentration gradient at the interface and δ as reference lengthscale (see Debray *et al.* [68] for a similar configuration).

Conversely, if the boundary layer is heavier than the bulk, a significant damping of the flow may be expected [69]. Both mechanisms have been experimentally observed [58, 70, 71, 34] in the vertical configuration; this may be related to the fact that δ is larger than in the horizontal case, since the convection levels are usually smaller. To conclude on this point, our opinion is that one should be aware of the limitations of the dilute alloy approximation.

3 Magnetic stabilization of unsteady growth

The use of a steady magnetic field has been of great benefit in the so-called "striation" or "solute banding" problem. Utech and Flemings [8] have demonstrated that a relatively weak DC magnetic field could eliminate these striations in 1966. In their paper, they remind us briefly about the principle of the formation of striations, put in evidence a couple of years earlier by Mueller and Wihelm [72]. Turbulence exists in the liquid pool due to the buoyancy forces and is responsible for temperature fluctuations. In particular the solid-liquid interface is submitted to such temperature fluctuations; this results in an unsteady growth rate and thus in bands of different concentration (see equation (25)). Their spacing is directly linked to the typical time scale of turbulent fluctuations through the mean growth rate. Let us also mention that, as discussed in section 2.4, unsteady convection can also interact directly with the solute boundary layer, resulting in striations (see equation (28)).

Utech and Flemings carried out growth experiments of tellurium doped indium antimonide in a horizontal Bridgman configuration, with different values of vertical DC magnetic field (0, 1750 and 1300 Gauss, corresponding to 0, 0.175 and 0.13 Tesla in the international unit system). They measured temperature fluctuations in the liquid in the absence of magnetic field, simultaneously with striations of the corresponding spacing in the solid. They observed no temperature fluctuations in the presence of vertical magnetic field (0.175 or 0.13 Tesla) nor did they find striations.

This problem of striations, of great importance for materials, is thus reduced to a pure fluid mechanics problem: magnetic stabilization. Subsequent studies have been devoted to a more systematic investigation of the conditions of stable convection under DC magnetic field in a

liquid metal or semi-conductor. The thermal driving force for a fully enclosed cavity is measured by a dimensionless Grashof number, $Gr = (\beta g G H^4)/\nu^2$, where β denotes the volume expansion coefficient, g gravity, G the typical temperature gradient perpendicular to gravity in the liquid, H the typical dimension of the pool and ν the kinematic viscosity. In the case where a free surface of liquid exists, an additional source of motion appears, the Marangoni convection. Surface tension is a function of temperature (the lower the temperature, the stronger is the surface tension in general) and temperature differences exist along the free boundary; the surface forces create a surface stream from high to low temperatures, recirculating in the bulk. The Marangoni number, $Ma = (\gamma G H^2)/(\rho \nu^2)$ is the dimensionless number measuring the strength of thermo-capillary convection. The symbol $\gamma = d\sigma_S/dT$ (where σ_S is the surface tension) denotes the temperature dependency of the surface tension (surface tension thermal coefficient). These two dimensionless parameters, Grashof Gr and Marangoni Ma represent the strength of buoyancy and thermo-capillarity versus viscous forces. Similarly, solutal Grashof and Marangoni numbers can be defined to account for composition driven bulk and surface convection. In most published papers, these effects are not taken into account (see section 2.5 for a discussion of the dilute alloy hypothesis).

Two other dimensionless numbers have to be considered, the Prandtl number $Pr = \nu/\alpha$, ratio of the kinematic viscosity to the thermal diffusivity and the Hartmann number $Ha = \sqrt{\sigma/(\rho\nu)}BH$, where σ is the electrical conductivity, ρ the density and B the magnitude of the magnetic field. The Hartmann number measures the relative importance of the electromagnetic forces to the viscous forces. In liquid metals, it is easily large compared to unity[1]. Liquid metals and semi-conductors are characterized by a low Prandtl number, of order 10^{-2}, depending solely on the thermo-physical properties of the liquid.

The basic problem is to find out the region of steady convection in the space of the parameters (Gr, Pr, Ha), with the addition of the Marangoni number Ma in the presence of a differentially heated free surface. In addition to these parameters, this problem depends on the configuration; geometry and orientation of temperature gradients, gravity and magnetic field. On the basis of common sense, and as confirmed by the analysis, an increase of the Grashof number (increase of driving force) or a reduction in the Hartmann number (reduction of the damping term) favour instability and therefore unsteadiness. The effect of a change in the Prandtl number on stability is less clear and was seen to depend on the configuration.

The dependence of the threshold of instabilities on the Hartmann number can take various forms, but it was often found that the required strength of the driving force (a Grashof number for instance) should increase as Ha^2. A tentative explanation can be given to the Ha^2 dependence of the threshold. An energetic argument is the following: the Joule dissipation is

$$\int_V \frac{\mathbf{J}^2}{\sigma} dV, \tag{32}$$

[1]Typically, the electrical conductivity is of order $\sigma \sim 10^6 \Omega^{-1} m^{-1}$, the kinematic viscosity scales as $\nu \sim 10^{-6} m^2.s^{-1}$, density as $\rho \sim 10^4 kg.m^{-3}$, which leads to $Ha \sim 10^4 BH$ (where B and H are expressed in Tesla and meter respectively). For a $10\,cm$ crucible size and $1\,T$, the Hartman number is of order 10^3.

whereas the viscous dissipation is

$$\int_V \rho\nu(\nabla \wedge \mathbf{V})^2 dV. \tag{33}$$

For the type of instability considered (transverse or longitudinal), rolls with axis perpendicular to the magnetic field are generated, which implies that the electric current density generated is of order σBV (only for rolls with axis aligned with the magnetic field, is the electric current density negligible compared to both the electrical potential gradient and electromotive force $\mathbf{J} \wedge \mathbf{B}$, see [73]). The ratio of the order of magnitude of Joule by viscous dissipation is found to be Ha^2. This suggests that the critical Grashof number should increase at the rate Ha^2. This approximate analysis is presented here only as a guiding idea and some of the assumptions (*e.g.* electrical current density of order σBV) may not hold in given circumstances. This stabilizing effect is directly linked to the microsegregation analysis developed in the previous section 2.4. The disturbance convective terms appear in the equations (25) and (28). Their reduction or cancellation has thus a direct effect on striations.

3.1 Vertical configuration

The vertical configuration, solidification starting from below, is the most widely used because it limits the thermal buoyancy driving forces, preserves in principle the rotational symmetry of the produced crystals and is generally solutally stable with the rejection of heavier material at the growing interface. Two sources of possibly unsteady convection exist: radial temperature gradients (always present, see section 4.1) and unstable vertical solute or thermal configuration (restricted to some alloys or to the top-seeded vertical Bridgman configuration). Some experimental studies reported the benefit of the use of a steady magnetic field to suppress striations associated with unsteady Rayleigh-Bénard convection [74, 75, 76]. Experiments have been carried out to measure temperature fluctuations under different magnetic field magnitudes and for a controlled temperature field. For instance, Kim [77] reports of an unstable Rayleigh-Bénard configuration, where a transverse magnetic field can be installed. He states that for a Rayleigh number of 0.9×10^5, a Hartmann number of 94 is enough to suppress temperature fluctuations. His interpretation is not very clear: the action of the magnetic field is described as an artificial increase of viscosity, which does not correspond to the physics of the Lorentz force.

More generally, as developed in [74], the physical interpretation is related to the stability analysis developed by Chandrasehkar [78]. The main result used is that in a Rayleigh-Bénard configuration, heated from below, with a vertical magnetic field, the critical curve is given in the $Ha - Ra$ plane by the relationship:

$$Ra_c = \pi^2 Ha^2 \tag{34}$$

The Rayleigh number is the product of the Grashof and the Prandtl number[2]. This result is valid for a magnetic field strong enough so that $Ha \gg 1$. Without magnetic field, and for no-slip boundary conditions, the critical Rayleigh number is 1708. So, only when the product πHa^2 is much larger than 1708, will the critical Rayleigh number follow this asymptotic behaviour.

[2] In the configuration heated from below, the dimensionless numbers Gr and Pr appear only in the product $Ra = GrPr$.

In the paper [74], Danilewsky *et al.* calculate the Rayleigh number associated to their growth configuration. In the case of the growth of Ga–As, a thermal Rayleigh number is relevant $Ra \sim 10^4$ and the $0.44\,T$ magnetic field is enough to suppress the striations. In the case of the growth of InP, the main buoyant forces are of solutal origin. The associated solutal Rayleigh number is much higher and the $0.44\,T$ magnetic field is not sufficient to eliminate striations. From the criterion, $Ra_c = \pi Ha^2$, the authors estimate that a $2\,T$ magnetic intensity should be required. In conclusion, when an unstable thermal or solutal gradient exists, the classical Chandrasekhar stability analysis seems to provide a good criterion for the stabilizing effect of a vertical magnetic field.

One difficulty appear when the field is not vertical but transverse. In Chandrasekhar's infinite plane configuration, the theory predicts that there should be no magnetic stabilizing effect, because the convection rolls after destabilization can have their axis aligned with the magnetic field. In this two-dimensional configuration, it is well-known that the Lorentz forces vanish (see Prof Moreau's contribution). Nevertheless, a magnetic stabilizing effect is observed [77, 79]. The reason for that is that the convection rolls must have a finite length along the transverse direction and this causes a breakdown of the two-dimensional state, which generates some electrical current and stabilizing Lorentz forces.

Rayleigh-Bénard instability is not the only possible source of time-dependence in the vertical Bridgman configuration. Indeed, even if the configuration is globally vertically stable, there exist some radial temperature gradients that will drive convective movements, without critical threshold. That convection can be itself unstable and lead to striations (see section 5.2 for a study case under rotating magnetic field).

3.2 Horizontal configuration

The horizontal Bridgman method is not the most widely used, but it is sometimes necessary for the growth of particular crystal like InP, CdTe, GaAs [4]. Its main advantage resides in the possibility of controlling the stoichiometry by a vapor pressure near the interface. This method is limited to high quality specific crystals. The horizontal Bridgman configuration received much academic attention, essentially on the point of view of the hydrodynamics, despite its restricted practical use. This is due probably to its extreme simplicity allowing for the development of analytical models.

3.2.1 State of the art without magnetic field

Historically, differentially heated fluids in horizontal cavities have received early attention regarding the stability of the convection (see experimental works [8, 80]). Such a configuration has been widely used to model horizontal Bridgman growth. In this case, a horizontal temperature gradient is setup and drives convection without any threshold value (see figure 4). In general, thermal and convective boundary layers can develop at both ends, but in the case of a long cavity or when thermal diffusivity is high (low Prandtl number fluids, like liquid metals) a fully-established parallel flow exists in the largest part of the cavity, characterized by the uniform axial thermal gradient $G = \Delta T/L$. For a "theoretical" two-dimensional cavity

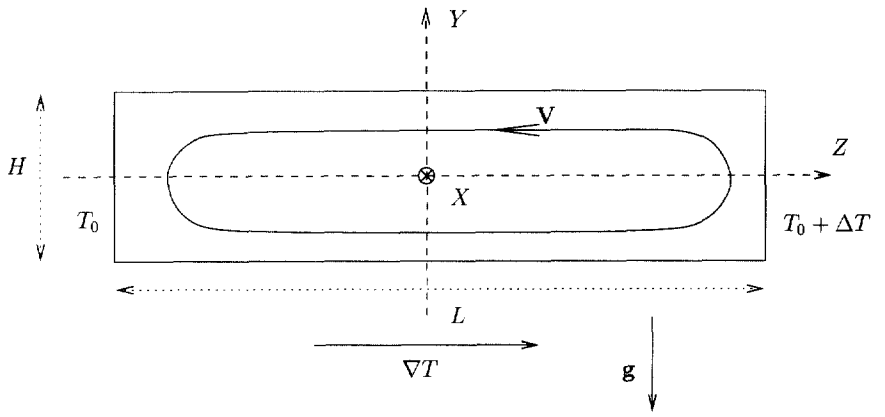

Figure 4: Horizontal Bridgman configuration

$(\partial/\partial X = 0)$, the basic flow and temperature field for thermally insulating upper and lower boundary conditions is [81, 82]:

$$W = \frac{\nu}{H} Gr \left[\frac{1}{6} \left(\frac{Y}{H} \right)^3 - \frac{1}{24} \left(\frac{Y}{H} \right) \right], \tag{35}$$

$$T = T_0 + \frac{\Delta T}{2} + GZ + [GrPr]\, GH \left[\frac{1}{120} \left(\frac{Y}{H} \right)^5 - \frac{1}{144} \left(\frac{Y}{H} \right)^3 + \frac{1}{384} \left(\frac{Y}{H} \right) \right] \tag{36}$$

A large number of studies have been devoted to the stability of this flow, analytically [82, 83, 84, 85], experimentally in configurations more or less equivalent to the situation described above [80, 86] and numerically [87, 88, 89]. In his pioneering work, Hart [82] identifies already the characteristic features of the possible instabilities. Basically, two types of instabilities are identified:

- Transverse instability: this instability is X-independent and corresponds to rolls with axis aligned along the X direction. The "linear" perturbation associated takes the form

$$\psi = e^{\sigma t}\, e^{k_Z Z}\, \hat{\psi}(Y), \tag{37}$$

$$\theta = e^{\sigma t}\, e^{k_Z Z}\, \hat{\theta}(Y), \tag{38}$$

  where ψ is a streamfunction in the Y-Z plane and θ is the temperature perturbation. At the threshold for this disturbance[3], it is found that the imaginary part of σ vanishes, which means that the linear disturbed state is steady: steady rolls are expected. Moreover, at small Prandtl number corresponding to liquid metals, the threshold is found to correspond to a critical Grashof number ($Gr_c \sim 7 \times 10^3$ [85]). This instability is interpreted as a shear instability of purely convective nature. Indeed, from the point of view of convection, the

[3]It is defined by the condition that the time growth rate becomes positive, or equivalently that the real part of σ is just zero.

basic flow is solely dependent on the Grashof number: its Reynolds number is proportional (with a pure constant of proportionality) to the Grashof number (see equation 35). Of course, the convective disturbance is very little affected by the temperature field, hence the Prandtl number, in the limit of low Prandtl numbers, because the temperature field becomes almost uniform in a cross-section (equation 36).

- Longitudinal instability: this instability is Z-independent and corresponds to rolls with axis aligned along the Z direction. The associated linear perturbation is of the form:

$$u_Z = e^{\sigma t}\, e^{k_X X}\, \hat{u_x}(Y), \tag{39}$$

$$\psi = e^{\sigma t}\, e^{k_X X}\, \hat{\psi}(Y), \tag{40}$$

$$\theta = e^{\sigma t}\, e^{k_X X}\, \hat{\theta}(Y), \tag{41}$$

where u_Z is the disturbance of the velocity in the Z direction, ψ the streamfunction of the disturbance in the X-Y plane and θ the temperature disturbance. At the threshold of linear instability, the imaginary part of σ is non-zero and the unstable linear disturbance takes the form of oscillating rolls, with an associated oscillatory temperature disturbance. This instability results from the coupling between buoyancy and temperature advection. The threshold value is not easily expressed in terms of the governing parameters Gr and Pr and is discussed below.

The neutral curves of stability are presented in figure 5 (these curves are reproduced from [84], figure 3 and correspond to the case of rigid thermally insulating upper and lower boundary conditions). The most interesting curves are labelled Tr and $Osc.$; they correspond respectively

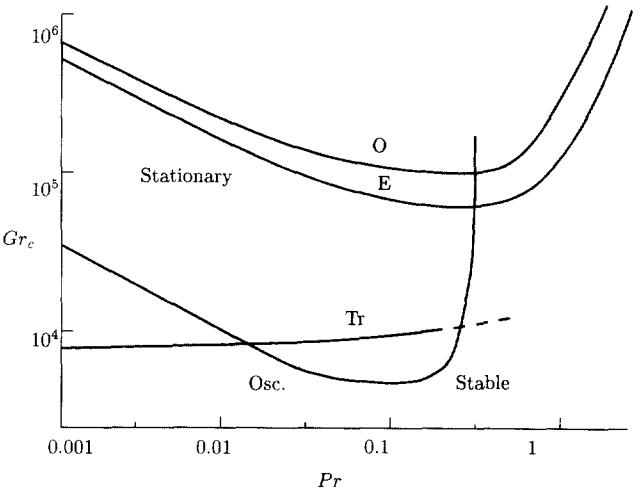

Figure 5: Neutral curves of stability in the Gr-Pr plane for thermally insulating boundaries, after Hart [84], JFM (1982), courtesy of the author and of Cambridge University Press.

to the transverse (steady) disturbances and to the oscillatory longitudinal disturbances. The

two other curves (O and E) correspond to stationary longitudinal modes.

Gill [83] gave a nice physical explanation for the onset of the longitudinal instability. The buoyancy-induced oscillatory torque in the X-Y plane driving the oscillatory rolls is provided by the oscillatory axial velocity disturbance u_Z that brings hotness or coolness according to the direction of u_x relative to the axial temperature gradient. He provides also, in the same paper, an approximate analytical stability analysis showing that, at small Prandtl number, a critical Rayleigh number $Ra = GrPr$ is relevant to account for the instability threshold of these longitudinal disturbances. More precisely, he indicates a critical value $Ra_c = 1030$. It is important to discuss this approximate analysis, to clarify exactly when this instability occurs. After his derivation of the critical value $Ra_c = 1030$, Gill discusses the approximations performed and concludes that the result may be valid for the case of perfectly thermally conducting shear-free upper and lower surfaces. Gill's approximate derivation assumes a uniform shear for the basic flow and a uniform vertical temperature gradient (which is reasonable in the middle part of the cavity $Y \simeq 0$, see equation 36). More important are the assumptions concerning the form of the disturbances eigenfunctions, which essentially correspond to perfectly conducting upper and lower walls (the disturbance vanishes at $z = \pm 1/2$).

Gill's theory is a success in two directions. First, it seems that it provides a good explanation for the experimental results of Hurle *et al.* [80]; they had noticed that the thermal disturbances had phase-surfaces aligned with the Z-direction. Secondly, in the case of thermally conducting boundaries, the theory agrees within a factor 2 with the numerical results of Hart [82] and criticality is associated to a critical Rayleigh number.

The limitations of Gill's theory are twofold. First, in the more physically relevant case of thermally insulating upper and lower boundary conditions, the numerical results [82, 84, 85] are not in agreement with the notion of a critical Rayleigh number at small Prandtl numbers. In the Gr-Pr plane, the neutral curve corresponding to the oscillatory longitudinal disturbances do not exhibit a -1 slope, which would correspond to a constant Rayleigh. At small Prandtl numbers, this slope seems to be close to $-1/2$, corresponding to a constant $GrPr^{1/2}$ product (see figure 5). So, in the general case, it is not appropriate to refer to the longitudinal instability as to a critical Rayleigh number. The $-1/2$ slope is an estimate from the numerical stability results, but no simple analytical theory, in the sense of Gill's theory, is available. The second limitation of the theory is that it assumes an infinite extent of the cavity in the X and Z directions. It has been shown that the finite extent of the cavity affects a lot the threshold of instabilities, by restricting the possible wave-numbers of the disturbances: it goes in the direction of stabilizing the flow (see the experimental work of Hurle *et al.* [80] and numerical studies [86, 87]).

An important point is whether transverse or longitudinal disturbances should be more particularly studied for liquid metals and the answer to this question depends on the Prandtl number. It was found that for a Prandtl number below 0.033 (Kuo and Korpela [90]), the first instability to appear was the (steady) transverse instability. As such, and because most liquid metal have a smaller Prandtl number, it was worth studying it. On the other hand, this first disturbance may just lead to steady rolls of weak amplitude, which would not explain the

appearance of temperature fluctuations responsible for the striations in crystal growth. For this reason, the longitudinal perturbations received much attention.

3.2.2 Influence of a magnetic field

Let us consider the same configuration with a vertical steady magnetic field. The dimensionless Hartmann number considered is obtained using the height H of the cavity $Ha = \sqrt{\sigma/(\rho\nu)}BH$. Experimental results [80, 91] and numerical results [92, 93] show an increase of the critical Grashof number (for a fixed Prandtl number) when the Hartmann number increases. More precisely it is reported in these studies that the critical Grashof number increases as the square of the Hartmann number. Taking into account the results of the previous section 3.2.1, we may conclude [93] that for thermally conducting boundary conditions, the neutral conditions are of the form:

$$GrPr \sim Ha^2, \tag{42}$$

whereas for thermally insulating boundary conditions , the neutral stability may take the form

$$GrPr^{\frac{1}{2}} \sim Ha^2, \tag{43}$$

This results concern the case of an electrically insulating crucible. Let us mention an adaptation of Gill's approximate analysis by Kaddeche (private communication) in the presence of a vertical magnetic field. He found that criticality was expressed as

$$Ra \sim Ha^2. \tag{44}$$

This analysis is believed to be appropriate for thermally conducting boundaries, in long and wide cavities and confirms the role of longitudinal disturbances.

Another characteristic of the magnetic field is that is seems to affect the steady transverse modes more effectively than the longitudinal modes. A consequence is that the value of the Prandtl number at which longitudinal disturbances become more unstable than transverse disturbances is reduced when the Hartmann number increases [93]. This gives more importance to the longitudinal disturbances when a magnetic field is present.

In a slightly different configuration (a horizontal cylinder), Davoust *et al.* [91, 94] found not only oscillatory longitudinal perturbations satisfying the Ha^2 dependence of criticality, but also an oscillatory transverse disturbance for which the critical temperature difference increases linearly with the Hartmann number.

Finally, it must be said that these studies are restricted to relatively small Hartmann numbers (of order 5), due to the numerical difficulty to increase the critical Grashof number or due to the impossibility to obtain a destabilization in experiments. This range ($Ha < 5$) is below the range where an asymptotic basic flow is reached under a strong magnetic field (see section 4.2). It may be suggested that the neutral conditions might take another form at high Hartmann number ($Ha > 100$), provided a huge Grashof number can be reached[4]. The behaviour

[4]This may be the case in the very different context of nuclear fusion, where an intense thermally driven convection in a liquid metal (the cooling fluid) is expected to take place under a strong magnetic field, in some proposed concepts.

of vortices in a strong magnetic field has been studied by Davidson [95].

Let us also mention a numerical linear stability under magnetic field parallel to the flow [92]. It has no effect on the basic flow, only on the disturbances. In this case the threshold value for the Grashof number is seen to increase linearly with the Hartmann number:

$$Gr_c = 115\,Ha. \tag{45}$$

4 The use of strong steady magnetic fields

The application of a steady magnetic field is not restricted to its ability to suppress unsteady convection. It is also used to decrease the steady convection level, with the hope to reduce the convective transport of species and to monitor macrosegregation at the scale of the whole crystal. Quite often unsteadiness is eliminated while there still exists a strong laminar flow that affects the solute layer thickness and segregation. An increase of the magnetic field magnitude will reduce that convection level and sometimes a purely diffusive regime can possibly be reached under normal gravity conditions [9].

Before the two typical vertical and horizontal Brigman configurations are considered, a general comment on the damping effect of a magnetic field on laminar convection can be made. It is well known that a magnetic field will reduce the convection magnitude: the total kinetic energy will be significantly less. It should be kept in mind that the flow structure[5] will change a lot as well. This is particularly important when the effects of convection on segregation are considered. As shown in section 2, only the velocity at the scale of the solute boundary layer thickness is relevant. Because of the change in structure of the flow under a strong magnetic field, it may well be that the total kinetic energy is significantly decreased while the velocity in the solute boundary layer remains unchanged [10]. Moreover, the question of the orientation of the magnetic field is crucial for the flow structure and magnitude depend critically on it.

Some simplifications will be used throughout this section unless otherwise specified, and are described here. The temperature inside the liquid region is determined from the energy equation. Numerical approaches consider both diffusion and convection heat transfer whereas the analytical studies assume that the relevant equation to be solved is simply:

$$\nabla^2 T = 0. \tag{46}$$

Such an assumption was found to be licit in many cases since the thermal Péclet number is often small. This is a simple purely diffusive thermal equation, with no heat source; the viscous dissipation is negligible for such low velocity movements of maximum order of magnitude of a centimeter per second and Joule dissipation is also negligible[6]. The MHD convection problem is then solved with the buoyancy driving force associated to the thermal field found from equation

[5]The term "flow structure" refers here to the occurrence of thin boundary layers or free shear layers and of an inviscid core region, when the Hartmann number $Ha = \sqrt{\sigma/(\rho\nu)}BH$ is very large compared to unity (see the first chapter on general MHD).

[6]Although these two dissipation modes are negligible in the thermal equation, they have been seen to play a key role in the kinetic energy equation in section 3.

(46). The non-linear inertial terms are neglected in the analytical studies, a safe assumption considering the small Reynolds numbers characteristic of such growth conditions. Furthermore, the magnetic field will reduce the convection level and will make even safer the assumption of negligible inertia. The set of equations to be considered is thus:

$$\nabla.\mathbf{V} = 0, \tag{47}$$

$$\nabla.\mathbf{J} = 0, \tag{48}$$

$$\mathbf{J} = \sigma(-\nabla\phi + \mathbf{V} \wedge \mathbf{B}), \tag{49}$$

$$\mathbf{0} = -\nabla p + \rho[1 - \beta(T - T_0)]\,\mathbf{g} + \mathbf{J} \wedge \mathbf{B} + \rho\nu\nabla^2\mathbf{V}. \tag{50}$$

Finally, concentration is determined from the convecto-diffusive equation (6) using the above mentioned global velocity field (convection and pulling velocity) and the boundary conditions at the boundary; zero normal gradient at the crucible and the solute rejection condition at the interface solid–liquid (equation (7)).

Another point is worth mentioning concerning inertia. In some references (*e.g.* [96]) the total velocity is calculated (buoyancy driven convection and global pulling rate in the reference system attached to the growing interface), while other authors (*e.g.* [56]) concentrate on the buoyancy driven flow and just add the uniform pulling rate to get the global velocity field (see figure 6). The difference between the *a priori* more exact former method and the more practical

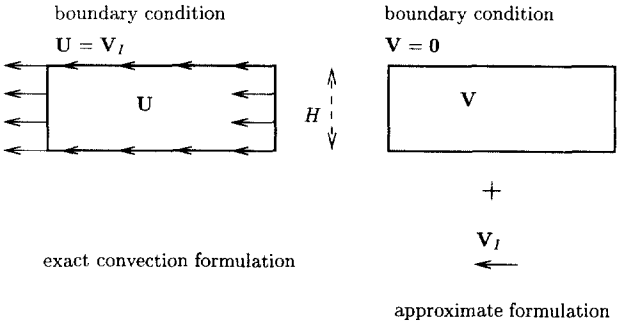

Figure 6: Exact and approximate convection problem formulation

later pertain to the influence of the single non-linear term in the dynamical equations, inertia. To our knowledge, the fact that these problems are different and the condition for them to be close to one another have not been discussed so far and we derive hereafter such a condition. The exact velocity solution $\mathbf{U}$ is split into the uniform pulling velocity and a pure convective part $\mathbf{U} = \mathbf{V}_I + \mathbf{V}$, and this expression is substituted into the Navier-Stokes equation for $\mathbf{U}$. The only difference between the equation thus obtained for $\mathbf{V}$ and the Navier-Stokes equation for $\mathbf{V}$ with the no-slip condition on the cavity walls is the following non-linear terms:

$$\mathbf{V}_I.\nabla\mathbf{V}_I + \mathbf{V}.\nabla\mathbf{V}_I + \mathbf{V}_I.\nabla\mathbf{V}. \tag{51}$$

The two first terms are strictly zero provided $\mathbf{V}_I$ is uniform. The last term can be compared to the viscous term $\nu\nabla^2\mathbf{V}$ using orders of magnitude. The most conservative hypothesis is to consider the length scale H, the diameter. The order of magnitude for $\mathbf{V}_I.\nabla\mathbf{V}$ is $V_I V/H$, while the order of magnitude of the viscous term is $\nu V/H^2$. The ratio is the Reynolds number based on V_I and H. The approximate problem gives a correct solution provided:

$$\frac{V_I H}{\nu} \ll 1. \tag{52}$$

Let us notice first that with a smaller length scale, the condition is more easy to fulfill (in that sense equation (52) is conservative) and secondly that this condition brings no constraint to the level of buoyancy-driven convection. This condition (eq. 52) is easily satisfied in crystal growth in general.

4.1 Vertical Bridgman configuration

The unavoidable radial thermal gradients near the solid-liquid interface always act as convection driving forces. Radial thermal gradients are most likely to develop in that region because the thermal conductivities of the solid and liquid are usually different: the redistribution of the essentially axial heat flux between the sample and the surrounding is accompanied by the appearance of radial thermal gradients (see figure 7). This radial flux is also responsible for a curvature of the interface[7]. Both effects, curvature and convection, will affect macrosegregation in general [35]. We shall concentrate on the segregation effect due to convection, since it will be directly influenced by a magnetic field, bearing in mind that a change in convection can counteract on the heat transfer and thus on the interface curvature. Quite generally, a variety of cases can be met depending on the position of the seed with respect to the melt, and on the density of the solute boundary layer with respect to the bulk fluid. However, the unavoidable radial thermal gradients near the solid liquid interface always act as convection driving forces.

Solute buoyancy forces also exist, due the rejection of solute rich material (if $k < 1$) into the fluid at the solid-liquid front. Generally, this is a stable configuration with rejection of heavier fluid. The stable solute buoyancy forces tend to damp the thermal buoyancy driven convection [58]. The other case (rejection of light material) could be catastrophic from the point of view of segregation, with all the solute being concentrated in the top end of the crystal; the vertical top-seeded configuration is then used but the thermal configuration becomes unstable.

4.1.1 Experimental macrosegregation results

Several teams report the influence of a strong steady magnetic field during vertical Bridgman crystal growth on solute segregation [76, 75, 9, 97, 98]. Under a transverse magnetic field of magnitude $0.4\,T$ [76], it was shown that the axial segregation diminished slightly while radial segregation increased during the growth of $In_xGa_{1-x}Sb$. Under a vertical magnetic field of magnitude $3\,T$, radial segregation was found to be significantly reduced [75] during the growth of $HgMnTe$. In the reference [9], the effect of a $3\,T$ vertical magnetic field on axial segregation in GaGe is presented. the authors express axial segregation in terms of the effective partition

[7]The orientation of the curvature shown on figure 7 corresponds to the case of a crystal of higher thermal conductivity than the liquid phase, a common situation for metals (opposite for semiconductors).

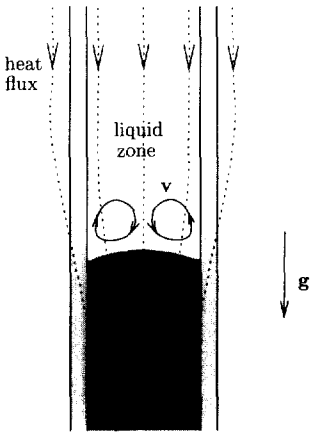

Figure 7: Vertical Bridgman configuration and its associated thermal convection pattern

ratio $k_{eff} = C_s/C_\infty$. The length of the crystal is less than the initial build-up length of the diffusive boundary layer. A fit of the experimental data with Tiller's expression [37] for the initial transient was accurate for an even lower diffusivity value than the accepted value in the literature, which proves that axial segregation corresponds to the pure diffusive regime. They report that radial segregation is negligible. Without magnetic field, the axial segregation was typical of a convective regime, with a steady-state effective partition ratio around 0.2 (the thermodynamic partition ratio is 0.087). Under the same circumstances, the application of an axial or transverse magnetic field up to $0.3\,T$ had no effect on the longitudinal segregation [99]. In the references [97, 98], the radial segregation in $HgCdTe$ is measured with no magnetic field and under an axial magnetic field of magnitude $5\,T$ respectively. In both cases, the axial composition obeys the pure diffusive distribution, whereas the radial segregation and the interface curvature are significantly less under $5\,T$ than without magnetic field. The relative radial segregation is changed from 47 % to 10 %.

All these results are compatible with a reduction in the convection level by a magnetic field, provided we keep in mind the behaviour of the response of axial and radial segregation to convection (see section 2). A schematic dependence of axial and radial segregation on the convection level is sketched in figure 8: the qualitative description of the experimental results is correct, based on the idea of a magnetic reduction of convection. In the next section 4.1.2, we shall come back to the results in reference [9] for comparison with a more precise modelling of the effect of the magnetic field.

4.1.2 Analysis of the fluid flow and its influence on segregation

General procedure

In the vertical Bridgman configuration under the presence of a magnetic field, the flow was investigated numerically [100, 96, 101, 102, 103] and received comparatively little attention on

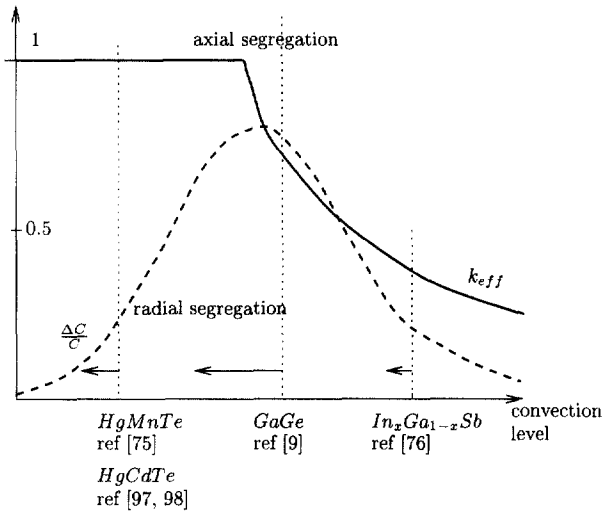

Figure 8: Axial and radial segregation in vertical Bridgman growth. The arrows show the reduction of convection level under the presence of a magnetic field

the analytical side [96, 104, 105]. The steps followed are essentially described below, except for reference [103] where a non-dilute alloy is considered and that we will discuss separately. First, an analytical temperature profile along the liquid boundary is chosen, as representative of the conditions of a real experiment. This temperature profile is not strictly axial and will induce radial temperature gradients in the liquid, which will drive the convection[8]. Secondly, the equations of motion (47,48,49,50) are solved using this temperature field. Thirdly, the effect of the velocity field on solute segregation is analyzed.

The axisymmetry of the configuration brings a simplification since the electrical potential can be proved to be uniform, when a vertical magnetic field is applied[9]. This is proved by taking the divergence of Ohm's law (49):

$$\nabla^2\phi = \mathbf{B}.(\nabla \wedge \mathbf{V}). \tag{53}$$

Since the buoyancy induced motion is purely meridional, this Poisson equation becomes a Laplace equation for ϕ (the term $\nabla \wedge \mathbf{V}$ is azimuthal), which solution is a constant under homogeneous boundary conditions. The Lorentz term $\mathbf{J} \wedge \mathbf{B}$ can be expressed directly in terms of the velocity:

$$\mathbf{J} \wedge \mathbf{B} = -\sigma B^2 \mathbf{V}_\perp, \tag{54}$$

[8]A deflection of the growth interface will result as well. This deflection, although generally neglected when convection is calculated, can have a direct effect on radial segregation [35].

[9]This is no longer valid when the axial symmetry is broken (*i.e.* with a transverse magnetic field) and the electrical potential ϕ must be determined.

where $\mathbf{V}_\perp$ is the part of the velocity field perpendicular to the vertical magnetic field[10].

Expected MHD features

The convective cells will be stretched along the magnetic field, to minimize the velocity gradient along the magnetic lines (*cf.* Prof. Moreau's contribution). In the case of a axial magnetic field, thin Hartmann layers are expected to develop along the solid-liquid front and along the opposite end of the liquid pool, while a thicker parallel layer will exist along the vertical crucible wall. Indeed, the following observations from numerical results are reported [101, 105]: when increasing the magnitude of the magnetic field, the convective loop initially located close to the solid-liquid interface where the radial temperature gradient is important is stretched until it reaches the whole length of the liquid region. The convective intensity decreases in the same time. It is also observed that the center of the convective loop moves towards the wall, so that the return path for the fluid becomes more and more narrow (see figure 9). The maximum intensity of the velocity is seen to decrease accordingly to the power law

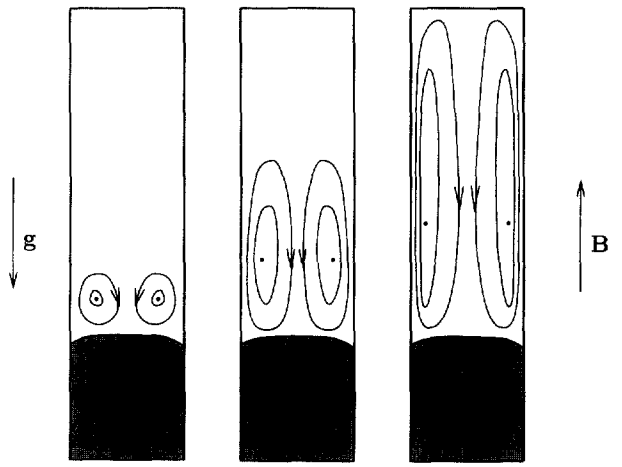

Figure 9: Stretching of convective loops in vertical Bridgman under vertical magnetic field.

$Ha^{-3/2}$ [101, 105]. In the reference [96], the power law found numerically is $\Psi_{max} \sim Ha^{-2}$ for the streamfunction, which will be found to be in agreement with the other references provided there exists a boundary layer of thickness $Ha^{-1/2}$. This is indeed the case along the crucible wall where a parallel layer develops and where all the flow recirculates (see next section).

Analytical MHD models

In 1988, Kim *et al.* [96], inspired by an analytical modelling of a Czochralskii configuration by Hjellming and Walker [106], proposed a simple MHD analysis of the flow at high Hartmann numbers. As described previously, they derive a temperature field $T(R, Z)$ from an almost

[10]The magnetic field does not necessarily need to be vertical and uniform. For the condition of vanishing electrical field to hold (and hence for equation (54) to be valid), **B** must be axisymmetric and poloidal.

linear temperature profile along the crucible wall with a small disturbance. They identify a core region and boundary layers (see figure 10). Although their final result is believed to be correct, some terminology mistakes should be underlined to place this paper in the usual context of MHD studies. The parallel layers (see figure 10) are called Hartmann layers (the correct typical thickness $Ha^{-1/2}$ is indicated) while the Hartmann layers are ignored and replaced by anonymous "end-regions". In this particular case of vanishing electrical field, it is allowed to ignore the Hartmann layers in the analysis because they do not carry a significant electrical current. Using the scale ν/H for velocity, H (diameter) for length and ΔT the temperature difference along the liquid for temperature, the curl of equation 50 takes the dimensionless form:

$$0 = Ha^2 \frac{\partial v_r}{\partial z} - Gr \frac{\partial \Theta}{\partial r} + \nabla^2 \omega_\theta, \tag{55}$$

where Θ is the dimensionless temperature and ω_θ the azimuthal component of dimensionless vorticity. A classical MHD result is that the last viscous term can compete only in Hartmann layers and parallel layers. In the core of the flow, there is an equilibrium between the thermal driving force and the Lorentz force. This leads to the core equation (equation (14) in reference [96]):

$$\frac{\partial v_r}{\partial z} = \frac{Gr}{Ha^2} \frac{\partial \Theta}{\partial r}. \tag{56}$$

As explained by the authors in reference [96], the no-slip condition is abandoned because the highest derivative term was dropped. Let us recall however that this method of transferring boundary conditions from the wall to the edge of the core flow appears simple here because the electric boundary condition is trivial[11]. This simplification is not universal in MHD and, in the presence of a non vanishing electrical field, the electrical boundary conditions for the core should be examined more carefully [107]: it is incorrect to assume an insulating condition $\mathbf{J}.\mathbf{n} = 0$ at the edge of a core region separated from an insulating wall by a Hartmann layer, since a high electric current can flow through the Hartmann layer. In [96], the dimensionless temperature field considered is given by the following equation:

$$\Theta(r, z) = [\epsilon z - C\epsilon z(1 - \epsilon z)] + \epsilon^2 \frac{C}{2}(1 - r^2) + \mathcal{O}(\epsilon^4), \tag{57}$$

where ϵ is the aspect ratio, diameter divided by the total length and C is a parameter describing the departure of the temperature field from the ideal purely axial heat flux. Using this temperature field, equation (56) can be easily integrated from the condition of vanishing radial velocity on the axis[12]. The other possibility followed in [96] is to introduce a dimensionless streamfunction ψ:

$$v_r = -\frac{1}{r} \frac{\partial \psi}{\partial z}, \tag{58}$$

$$v_z = \frac{1}{r} \frac{\partial \psi}{\partial r}. \tag{59}$$

Equation (56) becomes:

$$\frac{1}{r} \frac{\partial^2 \psi}{\partial z^2} = \frac{Gr}{Ha^2} C\epsilon^2 r. \tag{60}$$

[11] The azimuthal electric current and uniform electric potential satisfies an insulating or conducting boundary condition owing to the axisymmetry of the problem.

[12] Continuity is used to determine the vertical velocity.

The core solution, obtained from the condition of impermeable boundaries, is the following (to the leading order in ϵ):

$$\psi = -\frac{Gr}{Ha^2}\frac{C}{2}r^2\epsilon z(1-\epsilon z), \tag{61}$$

$$v_r = \frac{Gr}{Ha^2}\frac{C}{2}r\epsilon(1-2\epsilon z), \tag{62}$$

$$v_z = -\frac{Gr}{Ha^2}C\epsilon z(1-\epsilon z). \tag{63}$$

Typical isovalue curves of the streamfunction are shown on the left of the figure 10 and some velocity vectors on the right (note that vertical velocity is independent of the radius position in the core). Of course, the core flow recirculates through the parallel layer. The thickness of

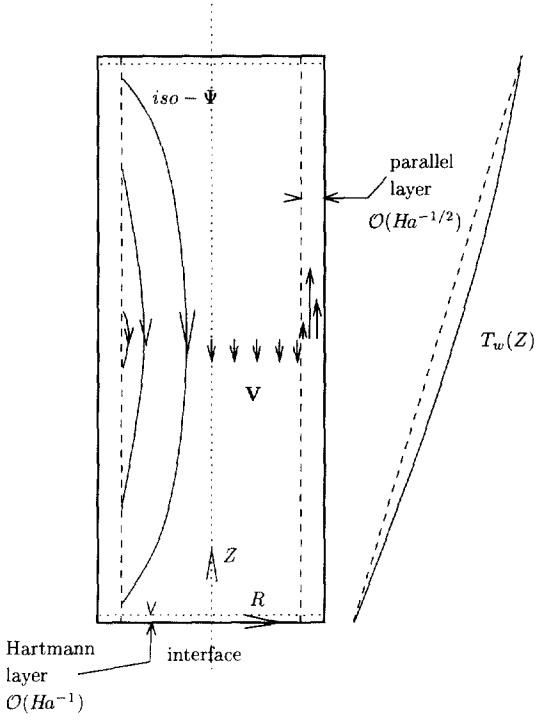

Figure 10: Asymptotic structure of the flow in vertical Bridgman under vertical magnetic field at high Hartmann number.

the parallel boundary layer has been assumed to be of order $Ha^{-1/2}$, without any reference to the aspect ratio. In fact, that magnitude order would be correct if the length reference was the length L. If we still keep the diameter H as the length reference, it is not difficult to derive that the parallel layer typical thickness $\delta_{||}$ should scale as:

$$\delta_{||} \sim Ha^{-\frac{1}{2}}\epsilon^{-\frac{1}{2}}. \tag{64}$$

From the solution (62) and (63), it can be seen that the velocity varies as Ha^{-2} in the core [96], and to be more precise, as $Ha^{-2}\epsilon$ for v_r and Ha^{-2} for v_z. From continuity, the upwards vertical velocity must vary as $Ha^{-3/2}$ in the parallel layer, and more precisely as $Ha^{-3/2}\epsilon^{1/2}$.

The previous asymptotic analysis was based on [96] (with differences in the non dimensional presentation). In [105], another similar analysis can be found for a different temperature field: the radial temperature gradients are supposed to be essentially located near the interface and decrease exponentially upwards. This temperature field is more realistic than the previous one and the analytical results are compared quantitatively with numerical simulations. Essentially, the same qualitative results are found, even if the temperature distribution is completely different: elongation of the convective cell, damping as Ha^{-2} in the core and $Ha^{-3/2}$ for the maximum of the velocity (in the parallel layer). It should be noted that the interface deflection has not been taken into account and the growing interface has been considered as flat in both studies.

An analytical segregation model

The originality of the analysis in [105] resides in that it does not stop after the determination of the asymptotic velocity field, but carries on with the segregation aspect. Starting from the expression of the velocity, an order of magnitude analysis of segregation is undertaken (based on equation (11) for axial segregation). The limit of convective regimes will be considered (convective velocity at the solute layer thickness scale being much larger than the pulling rate). Although the Hartmann layer has been seen to play no role in the determination of the asymptotic velocity field, two distinct cases have to be examined separately, the case when the solute layer is much thicker than the Hartmann layer and the opposite case when the solute layer is much thinner than the Hartmann layer.

When the Hartmann layer is much thinner than the solute layer, it is ignored and the scaling of the core region (*cf* equation (63)) is used: $-\overline{W}(\delta) \sim \frac{\nu}{H} GrHa^{-2}\frac{\delta}{H}$. In the convective regime, this leads to a solute layer thickness of magnitude order $\delta \sim H(GrSc)^{-1/2}Ha$ from equation (11). When the Hartmann layer is much thicker, the tangential velocity profile is linearized in the Hartmann layer and the normal velocity towards the interface is quadratic by continuity $-\overline{W}(\delta) \sim \frac{\nu}{H} GrHa^{-1}\left(\frac{\delta}{H}\right)^2$. The corresponding solute layer thickness is $\delta \sim H(GrSc)^{-1/3}Ha^{1/3}$. The limit between the two cases is found *a posteriori* from the result of the scaling: $Ha \sim (GrSc)^{1/4}$. If Ha is smaller than $(GrSc)^{1/4}$ the solute layer is included into the Hartmann layer, if it is larger than $(GrSc)^{1/4}$ the Hartmann layer is only a small part of the solute layer. This results are summarized in the following table 1.

A major conclusion of this segregation analysis under magnetic field is that the efficiency of the magnetic field in reducing segregation is not as impressive as its ability to reduce the velocity magnitude. This is particularly true when the solute layer lies within the Hartmann layer. In this region, the velocity gradient is not much smaller than in the absence of magnetic field and it is a key factor in the influence of convection on segregation.

The radial segregation can be addressed in the same asymptotic way. In reference [105], the radial segregation in the quasi-diffusive regime has been determined. The solute layer thickness is closed to the pure diffusive case D/V_I and the two cases to distinguish are $Ha^{-1}H < D/V_I$

	$\delta/H > Ha^{-1}$	$\delta/H < Ha^{-1}$
$-\overline{W}(\delta)$	$\frac{\nu}{H} Gr Ha^{-2} \frac{\delta}{H}$	$\frac{\nu}{H} Gr Ha^{-1} \left(\frac{\delta}{H}\right)^2$
δ	$H(GrSc)^{-1/2} Ha$	$H(GrSc)^{-1/3} Ha^{1/3}$
Δ	$Pe(GrSc)^{-1/2} Ha$	$Pe(GrSc)^{-1/3} Ha^{1/3}$
Validity	$Ha > (GrSc)^{1/4}$	$Ha < (GrSc)^{1/4}$

Table 1: Asymptotic axial segregation in the convective regime.

and $Ha^{-1}H > D/V_I$. The results are given here without proof:

$$if\ Ha < Pe, \qquad \Delta c/c \sim \frac{1-k}{1+kPe^2} Pe^{-1}(GrSc) Ha^{-1}, \tag{65}$$

$$if\ Ha > Pe, \qquad \Delta c/c \sim \frac{1-k}{1+kPe^2} (GrSc) Ha^{-2}, \tag{66}$$

Non-dilute alloys

Let us come back to the important case of non-dilute alloys (experiments [97, 98], numerics [103]), for which there exists a coupling between hydrodynamics and solute transport, invalidating the above decoupled analysis. The numerical analysis shows that there exists a strong stable solute stratification near the growing interface. It prevents any fluid particle from leaving that region. The thermal radial gradients can create a localized convection loop, but no global mixing can exist. The localized convective loop does generate some radial segregation. Since no global mixing of the fluid can exist, the axial solute segregation can vanish, provided the sample aspect ratio is small enough. The application of a very strong magnetic field can have an influence on the thermally driven convection, reducing its intensity and thus the radial segregation. The magnetic field has to be very intense, such that its effect is noticeable compared to the stratification damping [97, 98].

The reduction of the localized convective loop has another consequence: the solute gradient becomes steeper near the interface and this favours constitutional undercooling and polycrystalline growth. In addition, grains are generated ahead of the growth front. The grains formed are lighter than the melt in the reported experiments and move upwards by buoyancy, inducing a strong axial segregation [97]. In that case where the velocity field is strongly coupled with the solute field, no analytical solution has been proposed and only full numerical simulations are available.

4.2 Horizontal Bridgman configuration

The same approach is followed here as in the previous section 4.1. The flow is analyzed and the result used as an input for the order of magnitude analysis of segregation. The simplified two dimensional (2D) model is considered first, but we shall insist in section 4.2.2 that, in the

presence of a magnetic field, the 3D results can be totally different from the predictions of a 2D model depending on its symmetry. Section 4.2.3 is devoted to solute segregation results.

4.2.1 2D configuration

In a 2D model (in the vertical plane containing the growth direction), the geometry of the liquid zone is simply a rectangle and the buoyant driving force arises from the interaction of gravity and a horizontal (uniform) thermal gradient (see figure 11). The simplicity of the configuration prompted fundamental studies, because it was the configuration were analytical modelling from the flow to the species segregation seemed most promising.

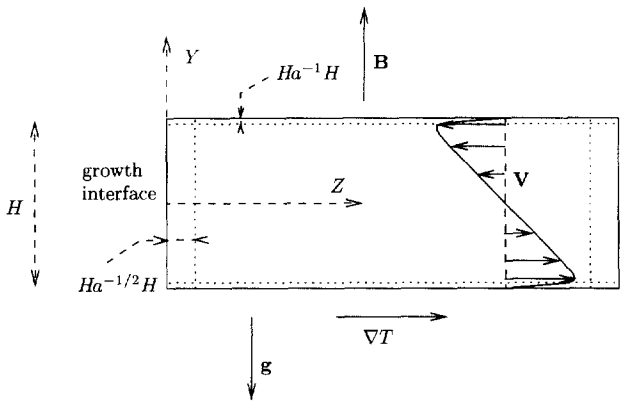

Figure 11: Ideal 2D horizontal Bridgman configuration

Although the experimental study on magnetic stabilization by Utech and Flemmings [8] dates back to 1966, the first attempt of modelling the damping of the steady flow is very recent [108]. The first step was to derive a fully-established analytical solution for the convection far from the ends of the liquids region in the 2D approach under a vertical magnetic field (figure 11). This 2D configuration is characterized by a vanishing electrical field (uniform potential field), like the axisymmetric vertical Bridgman with an axial magnetic field (see reference [108] for a proof). The parallel velocity profile found is the following:

$$W = \frac{\nu}{H}\frac{Gr}{Ha^2}\left[\frac{Ha\frac{Y}{H}}{2sh\frac{Ha}{2}} - \frac{Y}{H}\right], \tag{67}$$

the Grashof number being based on the axial uniform temperature gradient G, $Gr = (\beta g G H^4)/\nu^2$. This profile tends towards the linear profile:

$$W = -\frac{\nu}{H}\frac{Gr}{Ha^2}\frac{Y}{H}, \tag{68}$$

asymptotically when the Hartmann number is large. Hartmann layers on the upper and lower wall develop to satisfy the no-slip condition. This solution is identical for electrically insulating or conducting walls, due to the absence of electric field. The linear asymptotic profile can be

obtained directly from the curl of the Navier-Stokes equation (its single non zero X-component), when viscous action is neglected:

$$-\beta g \rho \frac{\partial T}{\partial Z} - \sigma B^2 \frac{\partial U}{\partial Y} = 0. \tag{69}$$

The term $\frac{\partial T}{\partial Z}$ is the axial temperature gradient G. The integrating of equation (69), with the global condition of no mass flux along the Z direction, leads to the linear profile (equation (68)). It must be insisted on the fact that this core solution was found without reference to the Hartmann layers, that play here a negligible role. Such a solution had been already found (Gershuni and Zhukovitskii [109]) in a different context and for a flow in the vertical direction under a transverse temperature gradient: this configuration has been seen to lead to the same fully-established solution.

The second result in reference [108] concerns the recirculation near the solid front. The solution is found in terms of a Fourier series. The result show that the recirculation takes place in a $Ha^{-1/2}H$ thin region (MHD parallel layer). This parallel layer, lies just in contact with the solid-liquid interface.

This results are confirmed numerically [110, 111, 93]. The work in reference [110], published before the analytical work [108], clearly displays the characteristics mentioned, linear core velocity profile and parallel recirculating boundary layers. In [111, 93], Alchaar *et al.* and Ben Hadid *et al.* compare explicitly their numerical solution to the analytic one, which they find accurate for high Hartmann numbers. Ben Hadid *et al.* also extend the study to the case of an upper free surface, an important practical case. It has to be noted that when inertial effects become important (high Grashof numbers), the computed solutions depart from the inertialess analytic solution.

4.2.2 3D configurations: analysis and experiments

After the discovery that buoyancy driven flows could follow a Ha^{-2} asymptotic law in terms of magnitude in a 2D cavity with insulating walls[13], the case of $3D$ cavities was investigated analytically [112, 107]. It was found that the asymptotic dependence of the flow magnitude is closely related to the global symmetry of the configuration for electrically insulating boundaries. A singular and a regular symmetry are defined (see figure 12). They are symmetries with respect to a plane $\mathcal{P}$, perpendicular to the magnetic field. These symmetries and their consequences are detailed mathematically [107], but they can be simply understood in terms of electrical current path. If the electrical current lines close themselves within the core of the flow (singular symmetry), the Lorentz damping is efficient and the flow magnitude scales as Ha^{-2}. If the current lines need to close in the Hartmann layers (regular symmetry), the resistance to the electric current is high, the Lorentz $\mathbf{J} \wedge \mathbf{B}$ force weak, and the flow magnitude scales as Ha^{-1}. The best result in terms of magnetic damping is associated to singular configurations. Unfortunately it is shown in [107] that a configuration without symmetry possesses the same characteristics as a regular configuration. More precisely, a configuration can be considered as singular only if

[13]The classical MHD result for pressure-driven flows in pipes is that the flow intensity decreases as Ha^{-1} when the wall are electrically insulating and Ha^{-2} when the walls are perfectly conducting [73].

the relative departure to the perfect symmetry is less than Ha^{-1}. In practice, great care must be taken to ensure a good symmetry of the geometry, temperature field and magnetic field.

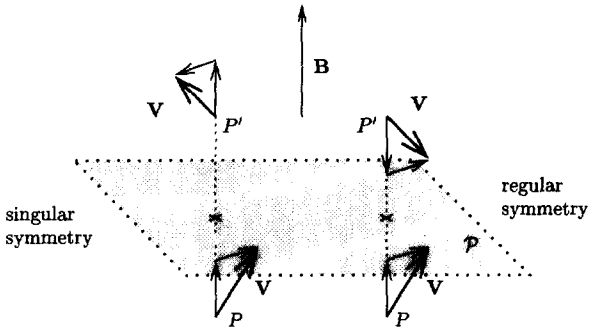

Figure 12: Singular and regular MHD symmetries

Some experimental results are available concerning the MHD damping of the flow [113, 114, 91]. The experiments reported in reference [114] show the importance of the symmetries mentioned previously. Convection in a cube is considered, the imposed temperature gradient is along the Z direction. The magnetic field has been applied along the three directions Z, X and Y in turn. When the field is applied along Z or Y (singular configuration), the measured heat transfer is reduced significantly when the magnetic field magnitude is increased. When the field is applied along X (regular symmetry), the effect of the magnetic field is much weaker. The figure 13 shows how the electric current flow depends on the nature of the symmetry. An alternative description of the effect of the magnetic field orientation is obtained from the electric potential equation, divergence of Ohm's law:

$$\nabla^2\Phi = \mathbf{B}.\mathbf{\Omega}, \tag{70}$$

where $\mathbf{\Omega} = \nabla \wedge \mathbf{V}$ is the vorticity field. The curl of the buoyant driving force, $\beta\rho\mathbf{g} \wedge \nabla T$ is identical in the three configurations in the figure 13 and parallel to X. In the case of singular symmetry, no significant electric potential is generated in the core, because $\mathbf{B}$ is essentially orthogonal to $\mathbf{\Omega}$. Close to the lateral walls, an electrical potential gradient is indeed necessary for the closure of the current lines, but such a gradient has no effect on the core flow. In the regular symmetry, $\mathbf{B}$ is parallel to $\mathbf{\Omega}$ and large electric potential difference are created: the electrical field almost compensates the electromotive force $\mathbf{V} \wedge \mathbf{B}$ in Ohm's law and a weak electrical current is generated.

The experiment described in [91] concerns buoyancy driven convection in a horizontal cylinder, modelling a Horizontal Bridgman configuration, under a vertical magnetic field. The temperature and electric potential have been measured. At high Hartmann number, the results are correctly predicted by the asymptotic theory [112]. This configuration is singularly symmetric and the velocity field decreases as Ha^{-2}. This configuration has been examined numerically [115, 116, 117]. The asymptotic results are confirmed and parallel layers are observed. The

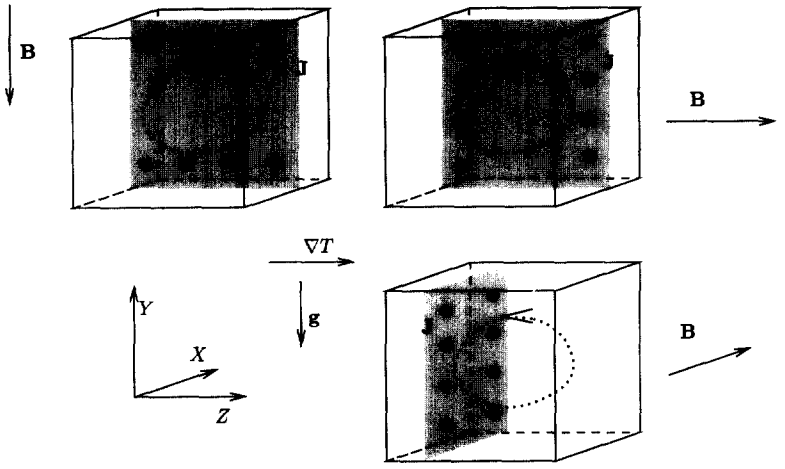

Figure 13: Convection in a cube (dashed line) under the three orientations for the magnetic field: the electromotive force ($\mathbf{V} \wedge \mathbf{B}$) through an arbitrary test plane (in grey) is indicated. It is zero on average for the Z and Y directions, and non-zero for the X direction. In this last case, an electric potential field is necessary to close the current lines; the electric current density and hence the Lorentz force are reduced.

most interesting to us lies along the solid-liquid front for future use in segregation models (see section 4.2.3). The vertical downwards velocity scales as $Ha^{-3/2}$ in this layer, by continuity.

4.2.3 Solute segregation

Solute segregation was studied numerically in this 2D horizontal Bridgman configuration under a vertical magnetic field [118, 119, 120]. Axial segregation is shown to decrease with increasing magnetic strength and radial segregation shows a maximum value for a moderate magnetic field. In the reference [120], Ma and Walker present an original idea: they consider that the flow is given by a Fourier series expansion and solve the solute segregation problem using the Lagrangian technique. The particles are tracked and diffusion is taken into account only within diffusion layers. In the core, the particles keep their concentration along their path. This method gives accurate results compared to a full numerical solution of the convecto-diffusion problem and the cost is significantly reduced in terms of computer resources.

The case of an axial magnetic field was studied experimentally and analytically in [10]. In this configuration, it is clear that the magnetic field has no effect on the parallel core flow. Nevertheless, the flow must recirculate near the solid-liquid interface (see figure 14). It was proved that the recirculating length must be of order HaH and that a Hartmann layer must exist between the recirculating region and the solid crystal. As a consequence, the flow was found to scale according to the following estimate outside the Hartmann layer:

$$W \sim -\frac{\nu}{H}\frac{Gr}{Ha}\frac{Z}{H}, \tag{71}$$

Such a velocity field was used to determine the segregation laws following the OMA analysis presented in section 2. It is valid only when the solute layer is much thicker than the Hartmann layer. The following results were found in the convective regime for axial and radial segregation:

$$\Delta \sim Pe\,(GrSc)^{-1/2}Ha^{1/2}, \tag{72}$$

$$\frac{\Delta C}{C} \sim (1-k)(GrSc)^{-1/3}Ha^{1/3}. \tag{73}$$

A weak dependence of axial segregation on the Hartmann number is found, with an exponent 1/2 only. Regarding radial segregation, its increase with the intensity of the magnetic field was to be expected, since the homogenization capacity of the flow is reduced (see figure 8). When the solute layer is contained in the Hartmann layer, an expression for the flow within the Hartmann layer must be used in the solute segregation analysis. Because the flow outside the Hartmann layer scales as Ha and the Hartmann layer thickness as Ha^{-1}, the flow in the Hartmann layer does not asymptotically depend on the Hartmann number. Consequently, the magnetic field is found to have no effect on segregation in this regime. The threshold between these cases is given by the relation $(GrSc)^{-1/3}Ha \sim 1$. For Ha less than $(GrSc)^{1/3}$ no effect of the magnetic field is expected and for larger Hartmann numbers, the laws (72, 73) apply. These analytical predictions were also confirmed numerically and experimentally in [10]. The experiments consisted in measuring the axial segregation along $\Phi 6\,mm$ samples of the SnBi alloy grown under axial magnetic fields between 0 and $1.3\,T$, corresponding to Hartmann numbers between 0 and 270. The magnetic field had no effect for weak magnetic fields and a small effect of reduction of axial segregation for larger magnitudes.

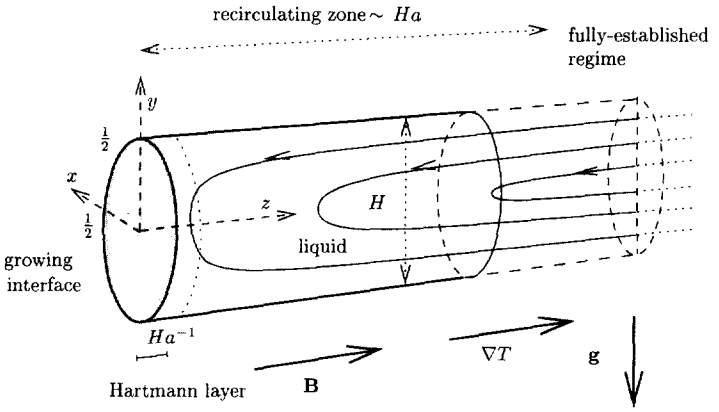

Figure 14: Horizontal Bridgman configuration under axial magnetic field

Segregation in a horizontal Bridgman configuration under a vertical magnetic field is now examined. An analytical solute segregation model has been developed in this case [121, 105]. In the convective limit, two regimes are found depending on the relative value of Ha and the product $GrSc$:

$$if\ Ha(GrSc)^{-2/5} < 1, \qquad \Delta \sim Pe\,(GrSc)^{-1/3}Ha^{1/3}, \tag{74}$$

$$if\ Ha(GrSc)^{-2/5} > 1, \qquad \Delta \sim Pe\,(GrSc)^{-1}Ha^2, \tag{75}$$

The regimes depend again on the relative thickness of the dynamical (parallel) and solute layer. When the field is vertical, its effect on segregation is much stronger than that found under an axial field.

4.2.4 Some remarks

A point was made clear during the experiments described in [91]: even if the Hartmann number is significantly larger than unity (around 100), the temperature field is not necessarily close to the pure diffusive profile. There is a need to examine buoyancy-driven convection at high Hartmann number and very high Grashof number. The magnetic field is strong enough to modify the flow structure and intensity, but interacts with the temperature field non linearly. This point has received attention on a theoretical point of view [122]. New MHD boundary layers can form and have an influence on the global flow. This area should be examined more carefully because of its potential relevance to the study of non-dilute alloys.

In the micro-gravity environment, the Bridgman technique has received comparatively more attention than on earth, because of the inapplicability of the Czochralskii method. Even under $10^{-4} - 10^{-5}g$, the solute diffusive regime is very difficult to obtain and it has been suggested that only the combination of μg and Lorentz damping could provide the conditions of pure diffusion during crystal growth. This has prompted a number of studies concerning the damping of the flow [123, 124, 119]. More generally, this configuration is close to the earth-based horizontal technique: the random $g - jitters$ have axial and transverse components relative to the crystal. The transverse components interact with the imposed axial gradient and are more likely to generate most of the buoyant convection.

To conclude this part 4, let us emphasize two aspects of the use of strong magnetic fields during crystal growth:

- A magnetic field reduces strongly the intensity of the buoyancy-driven convection. The efficiency of the magnetic damping depends highly on the symmetry of the configuration. In vertical Bridgman growth, the field should be axial to obtain an efficient damping (the Ha^{-2} regime), whereas in horizontal Bridgman growth, the magnetic field should be vertical. The whole symmetry (geometry, magnetic field, thermal field) must be precisely controlled at high Hartmann number for the Ha^{-2} damping law to hold.

- The efficiency of the magnetic field in reducing the convective effects on solute mass transfer is not as high as expected from the reduction in velocity. This is due essentially to the formation of thin boundary layers under a strong magnetic field: the velocity gradients near the solid-liquid interface do not decrease so rapidly when increasing the magnitude of the magnetic field and when the solute boundary layer is totally included into the MHD layer, the only important convective parameter is the velocity gradient at the solid-liquid interface.

5 Rotating magnetic fields

5.1 Introduction

The topic being addressed in detail in other contributions to the present handbook, we shall here only recall briefly the characteristic features of the flow driven by a rotating magnetic field. In a typical Bridgman configuration, the furnace can be inserted within the stator of a standard motor fed by an AC electric current of typical frequency 50 Hz. In most cases, the hydrodynamic velocity is very small compared to the field rotation rate. As a consequence, the magnetic problem can be solved first, assuming the fluid to be at rest (rigid rotor approximation), and the field thus derived used as an input in the Navier-Stokes equation.

The magnetic field lies principally in the radial direction and the Lorentz force $\mathbf{J} \wedge \mathbf{B}$ as well as the primary flow are thus mainly azimuthal. However, due to no slip conditions at the solid-liquid interface, a secondary flow is driven by the axial variation of the core pressure gradient (Ekman pumping), resulting in a meridional motion. The Ekman circulation was found to govern the scaling of the whole flow, including the azimuthal component, by providing energetic and angular momentum equilibrium relationships (see Davidson and co-workers [125, 126]). As shown in a recent study [127, 128], the non dimensional numbers governing the hydrodynamic field in an isothermal fluid are :

- the aspect ratio of the fluid column, $\epsilon = H/L$
- the screening parameter, $R\omega = \mu\sigma\omega H^2/p$
- the magnetic Taylor number, $Tm = \sigma\omega B^2 H^4/2p\rho\nu^2$

In the above expressions, $\omega = 2\pi f$ is the pulsation of the AC current, p the number of pair of poles, the other symbols being defined previously. The screening parameter $R\omega$ is a measure of the penetration of the magnetic field within the fluid, whereas the magnetic Taylor number measures the relative efficiency of inertia and/or viscosity in balancing the driving action of the rotating field. As such, it is similar to the Grashof number met in natural convection problems, with the Lorentz force replacing buoyancy.

Using typical values for the magnetic permeability $\mu = 4\pi\ 10^{-7}$ H/m, the electrical conductivity $\sigma = 2\ 10^6\ \Omega^{-1}m^{-1}$, the pulsation $\omega = 100\ \pi$, a number of poles $p = 1$ and a cavity radius $H = 2.5\ cm$, we get $R\omega \simeq 0.5$. If we take in addition a mass density $\rho = 10^4\ \mathrm{kg.m^{-3}}$, a kinematic viscosity $\nu = 3\ 10^{-7}\ m^2s^{-1}$ and a magnetic field $B = 10^{-3}\ T$, we find $Tm \simeq 1.4\ 10^5$.

In most laboratory scale experiments, the magnetic field can thus be assumed to penetrate fully in the liquid sample. Nevertheless, a significant skin effect can not be excluded at higher frequencies and/or cavity dimensions. As for the high value of the Taylor number, the conclusion is that the hydrodynamic problem is characterized by a balance between inertia and the Lorentz force. In dimensional terms, the typical fluid velocities will thus scale as :

$$V_0 = BH(\sigma\omega/2p\rho)^{1/2} \tag{76}$$

One should be aware that the above expression is only valid as a first approximation. As a matter of fact, in steady flows, the characteristic velocity of the primary azimuthal motion is a factor $Tm^{1/6}$ higher than V_0, whereas the secondary meridional flow has a typical velocity $Tm^{1/6}$ lower than V_0 [125, 127, 128]. In the turbulent regime, the correcting factors are in $Tm^{1/18}$ instead of $Tm^{1/6}$ [125, 127, 128], or can take the form of a dimensionless friction factor [11, 129]. In any case,from a crystal grower point of view, equation (76) can be considered to capture the essential physics of the hydrodynamic problem. In crystal growth configuration, the estimate of equation (76) should be compared to a typical natural convection velocity to identify the leading heat and mass transport mechanism.

It should also be mentioned that the flow driven by a rotating field can become unstationary when the driving force, measured by the magnetic Taylor number exceeds a given threshold. A Taylor-Couette mechanism can be invoked to account for the development of the instability, which is of course very much dependent of the aspect ratio of the cavity [130]. From the stability analysis carried out by Richardson [131], the Tm threshold was found equal to 2917 for an infinite fluid, but the critical Tm number is higher than $3\ 10^5$ for a cavity of aspect ratio $\epsilon = 1/2$ [130]. More precisely, the effect of containment was studied in detail in the numerical study of Kaiser and Benz [132].

5.2 Steady / unsteady flow

In a cylindrical cavity heated from below, the motion driven by rotating magnetic fields can easily overwhelm Rayleigh-Bénard type convection. Such a result was clearly observed in the experiments of Dold and Benz [11, 133] on liquid gallium, where the rotating field had a frequency of $50Hz$ and an intensity ranging from 0.2 to 30 mT. The temperature fluctuations associated with the initially unsteady flow were of the order of $\Delta T = 1\ K$, with a characteristic frequency in the 0.01 to $0.1Hz$ range when no magnetic field was applied.

On the other hand, as soon as B exceeded $0.6\,mT$, ΔT was reduced by approximately one order of magnitude [11]. Using the experimental parameters and the thermophysical properties listed in ref. [133], the Taylor number associated with $B = 0.6\ mT$ is $Tm = 1.7\ 10^5$; for a cavity of aspect ratio $\epsilon = 1/2$, this result is thus a fair agreement with existing numerical [127, 128] and experimental [130, 134] data. Besides, the remaining temperature fluctuations were of much higher frequency, typically in the Hz range, and could be associated with the convection velocity driven by the rotating field.

Indeed, the frequencies measured at $B_1 = 5.6\ mT$ ($f_1 = 1.1\ Hz$) and at $B_2 = 10\ mT$ ($f_2 = 2\ Hz$) [133] are exactly in the ratio of the magnetic inductions, $f_2/f_1 = B_2/B_1$, which can be understood by the fact that the convective velocity is directly proportional to the intensity of the rotation field. (see eq. (76)). Another interesting observation was that the temperature fluctuations observed in an initially stable thermal configuration (*i.e.* heated from above) are similar at a magnetic induction $B = 10\ mT$, demonstrating that the temperature field only depends on the rotating field driven convection [11].

These findings were confirmed by Bridgman growth experiments of gallium doped germanium [11] crystals. In the top seeded configuration, equivalent to the heated from below Rayleigh-Benard problem, both the intensity of the dopant striations and their spacings were reduced upon application of the rotating field. On the other hand, in the classical bottom seeded configuration, a rotational sriation pattern is generated when the magnetic induction exceeds the threshold value.

Similar results were obtained by Friedrich *et al.* [12], for both a model liquid gallium cell heated from above and gradient freeze growth experiments, again on gallium doped germanium. In addition, numerical simulations were performed, that showed a good agreement with the experimental data. The gallium cell had an aspect ratio $\epsilon = 1/2$, and temperature fluctuations were seen to appear when the magnetic field exceeded $B = 1.1\ mT$, independently of the imposed stabilizing temperature difference.

Using once more the thermophysical properties listed in ref. [133], $B = 1.1\ mT$ corresponds to a Taylor number $Tm = 3.8\ 10^6$. Such a value is somewhat higher than those previously reported, but one should not forget that the interpretation of the experimental results is quite sensitive to the choice of thermophysical properties. In any case, the problem of flow destabilization under the action of a rotating field should still be considered open for research.

The mechanism of flow stabilization in an initially unsteady vertical Bridgman configuration was studied in some detail in the numerical simulations of Marty *et al.* [135]. In a cavity of aspect ratio $\epsilon = 1/2$, an instability was seen to occur when the Grashof number based on the radial temperature difference at the interface exceeded $3.2\ 10^6$. Such an instability was clearly associated with the inflexional nature of the velocity profile in the convective loop.

Upon application of a rotating magnetic field, for the case where the secondary meridional motion is opposite to the buoyancy driven flow in the vicinity of the interface, the temperature and velocity fluctuations in the melt were found to disappear at a value of the Taylor number $Tm = 3400$. As the jet Reynolds number is reduced, stable conditions can be restored thanks to the rotating field [135].

Such a conclusion was further confirmed by the fact that when the meridional motion and the buoyancy driven convection are in the same direction in the vicinity of the interface, the critical Grashof number necessary to destabilize an initially stable flow is reduced [135]. Depending on the thermal configuration, a rotating magnetic field may thus be ineffective in damping natural convection instabilities.

5.3 Heat and mass transfer

The first effect of the rotating magnetic field is an uniformization of the temperature and the composition along the azimuthal direction, due to the strong primary motion. Such an uniformization can be considered beneficial, as it smoothes out undesirable temperature and composition heterogeneities; however, it may also induce rotational striations [12] in a thermally

heterogeneous environment. However, in terms of heat and mass transport, it is the secondary flow that will most impact on the quality of the grown crystals.

Indeed, a significant modification of the interface shape as a function of the magnetic induction was observed by both Dold and Benz [11] and Friedrich *et al.* [12] in their experiments on gallium doped germanium. Such a result can be understood by the fact that the classical thermal Peclet number may take values significantly higher than unity, even in a good heat conductor such as molten germanium, when the rotating field is turned on. The secondary convective motion was shown to acccount for the "w" shape of the growth interface [12].

The rotating magnetic field was seen to have no effect on the axial composition profiles, since the buoyancy driven flow is strong enough to control species transport [12]. In other words, in the experiments of Friedrich *et al.*, the effective and equilibrium partition coefficients (see equation (15)) were very close even at $B = 0$. However, for other growth conditions, the increase of the meridional fluid velocity associated with the secondary action of the rotating field may have an impact on axial segregation.

A significant improvement in terms of radial composition homogeneity at magnetic inductions of $B = 1.3\ mT$ and $B = 4.4\ mT$ was also observed in the experiments of Friedrich *et al.* [12]. Such a finding was understood as an effect of the increased flow velocity in the vicinity of the interface, that led to a better mixing of the melt. However, the reduction of radial segregation was obtained at the expense of a loss in tems of microscale concentration variations, as the rotating field generated striations in the grown crystals.

6 Other magnetic effects

6.1 Thermoelectricity

The possible influence of thermoelectric magnetohydrodynamic (TEMHD) effects on fluid flow has been recognized dating back to the pioneering works of Shercliff [136] and Gel'fgat and Gorbunov [137]. In the field of Bridgman crystal growth, the problem was recently studied in detail by Khine and Walker, and our presentation is principally based on their work [138, 139]. The physical basis for TEMHD effects is the existence of an additional contribution to the electric current density in a material of absolute thermoelectric power S submitted to a temperature gradient ∇T, namely :

$$\mathbf{J} = \sigma(-\nabla\phi + \mathbf{V} \wedge \mathbf{B} - S\nabla T). \tag{77}$$

Provided that the cross product $\nabla T \wedge \nabla S$ is different from zero[14], the static electric field can not balance the thermoelectric contribution and a current will run through the material. Such a current will interact with an imposed magnetic field and drive some fluid flow. In refs. [138, 139], an axial magnetic field was considered and the relevant temperature gradient is directed radially along the solid liquid interface; their interaction leads to a principally

[14]It should be noted that if S is a function of temperature only, then this product $\nabla T \wedge \nabla S$ vanishes [136].

azimuthal convective motion. Denoting ΔT_R the characteristic temperature difference, the radial thermoelectric current density scales as [140] :

$$J = \frac{\sigma \Delta S \Delta T_R}{H}, \tag{78}$$

where ΔS stands for the difference in thermoelectric power between the solid and liquid phases and H for the radius of the sample. If the Lorentz force $\mathbf{J} \wedge \mathbf{B}$ is balanced by viscosity, a characteristic value of the azimuthal convective velocity can be written as :

$$V_\theta = \frac{\sigma \Delta S \Delta T_R B H}{\rho \nu}. \tag{79}$$

On the other hand, if the flow is not governed by viscosity, V_θ will increase until $\mathbf{V}_\theta \wedge \mathbf{B}$ is the dominant term in the current density. Comparison with eq. (78) then yields :

$$V_\theta = \frac{\Delta S \Delta T_R}{B H}. \tag{80}$$

Since the Hartmann number measures the relative importance of electromagnetic forces and viscous stresses, the transition between the ranges of validity of eqs. (79) and (80) should occur around $Ha \cong 1$. The above scaling laws were verified experimentally in the work of Gel'fgat and Gorbunov [137] where the authors observed the fluid velocity to be proportional to B(resp. B^{-1}) at low (resp. high) magnetic inductions.

It should be recalled that natural convection velocities scale as either B^{-2} or B^{-1} depending mostly on symmetry considerations. Equation (80) shows clearly that TEMHD effects may be dominant at high magnetic fields provided natural convection follows the B^{-2} power law. Taking once more characteristic values of thermophysical properties of liquid metals and semiconductors, $\sigma = 2 \times 10^6\ \Omega^{-1}m^{-1}$, $\rho = 10^4\ \mathrm{kg.m^{-3}}$, $\nu = 3 \times 10^{-7}\ m^2s^{-1}$, and setting $B = 0.1\ T$, $H = 0.01\ m$, $\Delta S = 10^{-5}\ VK^{-1}$ and $\Delta T_R = 1\ K$, we get $Ha = 25$, and eq. (80) yields $V_\theta = 0.01\ ms^{-1}$. One should thus be aware that a relatively modest temperature difference along the interface can drive a fairly rapid azimuthal motion.

As noted in section 5 for the rotating field problem, such an azimuthal motion may lead to rotational striations if the growth environment is not perfectly axisymmetric. Such striations were experimentally observed by Cröll *et al.* [141] in float zone growth of doped silicon crystals. Besides, an excessive azimuthal velocity may lead to Taylor-Couette type hydrodynamic instabilities. However, the magnetic fields necessary for the observation of TEMHD effects are often quite high ($Ha \gg 1$) and should thus be efficient in the damping of fluctuations.

Another formal similarity with the rotating field problem can be found, namely that the primary azimuthal flow drives a secondary meridional motion. Indeed, the centrifugal force can only be balanced by a pressure gradient if V_θ is independent of the axial coordinate Z. More precisely, it can be shown that the governing equation for meridional motion features a forcing $V_\theta\, \partial V_\theta / \partial Z$ term [138].

An estimate for the characteristic value of the meridional velocity can be obtained by writing a balance between the pressure gradient associated with the azimuthal flow, and, depending

on the magnitude of the Hartmann number, either the viscous stresses or the Lorentz force of the meridional flow. For instance, in the usual case where *Ha* is larger than unity, equating $\rho\, V_\theta^2\, /\, H$ and $\sigma\, V_M\, B^2$ yields for the meridional velocity :

$$V_M = \frac{\rho \Delta S^2 \Delta T_R^2}{\sigma H^3 B^4}. \tag{81}$$

Using the numerical values listed in this section, we get $V_M = 5\ 10^{-3}\ ms^{-1}$. Such a convection velocity can clearly have an impact on mass transport in the melt, and thus on solute segregation, specially at low growth rates (see *e.g.* eq. (11)). However, due to the B^{-4} dependence of V_M, a higher magnetic field will result in a much reduced meridional velocity [138], so that no general conclusion can be drawn on this point. To sum things up, it appears that thermoelectric effects must never be *a priori* neglected, since they can have a significant impact on the growth process.

Finally, an important practical point lies in the electrical nature of the crucible. If the latter is electrically conducting (graphite is sometimes used), and since its absolute thermoelectric power is likely to differ from that of the liquid, the imposed axial thermal gradient will drive a strong thermoelectric current and hence a strong convection when a magnetic field is applied. The temperature difference involved being much larger then the temperature difference on the solid-liquid surface, this motion would dominate the above-mentioned convection. The use of an electrically insulating crucible material eliminates this effect.

6.2 The magnetic force and its consequences

Apart from its coupling with conduction electric currents (essentially due to the movement of the free electrons), the magnetic field can have a direct effect on the atomic structure (essentially on the electrons linked to the nucleus) which generates a magnetic moment that interacts with the background magnetic field. This results in a force density, the "magnetic force", independent of the Lorentz force $\mathbf{J} \wedge \mathbf{B}$. A striking example of the magnetic force is ferromagnetism. Nevertheless, we shall not be interested in ferromagnetism since it does not concern liquids nor high temperature solids above the Curie point. Even the so-called non-magnetic materials are slightly magnetic and the magnetic moment density field $\mathbf{M}$ takes the general expression [142]:

$$\mathbf{M} = \chi_m \mathbf{H}, \tag{82}$$

where χ_m is called the magnetic susceptibility of the material and $\mathbf{H}$ is the magnetic field[15]. For ferromagnetic magnetic materials, χ_m would be of order unity and positive. For most non-magnetic, diamagnetic materials, χ_m is slightly negative ($\chi_m \sim -10^{-6}$) and for some others, paramagnetic materials, it is slightly positive ($\chi_m \sim 10^{-4}$). The density of force, per unit volume, associated to the magnetic moment (82), can be written:

$$\mathbf{F} = \frac{\chi_m}{2\,\mu_0} \nabla \left(\mathbf{B}^2\right). \tag{83}$$

[15]The magnetic field $\mathbf{H}$ is defined from the magnetic induction $\mathbf{B}$ and the magnetic moment field $\mathbf{M}$ by the relation: $\mathbf{H} = \mathbf{B}/\mu_0 - \mathbf{M}$, where $\mu_0 = 4\pi 10{-}7H/m$ is the vacuum magnetic permeability. In practice, because χ_m is so small, of order 10^{-6} for diamagnetic materials, we can assume that the magnetic field is undisturbed by the magnetic moment density created. By abuse of language, we also call $\mathbf{B}$ the magnetic field.

As can be seen in this expression, only the gradient of magnetic field produces some force. In spite of the very small value of χ_m for non magnetic materials like water or wood, these materials can be levitated in a strong magnetic field gradient [143]. Magnetic fields of order $10\,T$ varying over a distance of order $10\,cm$ are necessary.

Magnetically-driven convection

A buoyancy driven flow in a non-uniform magnetic field is subjected to the magnetic force (83). Depending on the arrangement of the imposed magnetic field, buoyancy can be enhanced or reduced. Braithwaite *et al.* [144] considered a Rayleigh-Bénard configuration using a electrically insulating liquid with a magnetic force upwards and downwards respectively. In the first case the Nusselt number is increased and in the second case, it is decreased. With a strong enough downwards magnetic force density, they report that convection is suppressed and the diffusive temperature field is observed (Nusselt is unity). This effect arises because the magnetic susceptibility depends on temperature; indeed, if χ_m were uniform, the magnetic force could just be equilibrated by a pressure gradient. With the variation of χ_m with temperature, the magnetic force becomes analogous to the buoyant force, for which the density variations with temperature result in a net torque causing convection after some threshold. Because the magnetic force was able to cancel the effects of ordinary buoyancy forces, they have been referred to as anti-gravity forces[144].

In crystal growth relevant configuration with an electrically conducting liquid, both the magnetic force (83) and the Lorentz force should be taken into account. The order of magnitude of each force should be estimated, bearing in mind that only the variations of χ_m will produce a motion.

Effects on micro-structures

A strong uniform magnetic field can have an influence on the structure of polycrystals. The effects are quite complex and their interpretation is still unsure. However it seems that they can be divided into two categories: the effect of a magnetic field on the conditions of homogeneous nucleation and the orientation effect of the magnetic field on the small crystals. Under a $3.5\,T$, it was reported [145] that nucleation was enhanced in comparison with the case of no magnetic field. The explanation involves energetic considerations from the appearance of a crystal nucleus and the effect of the magnetic field. Other studies with weak magnetic field show no change due to the application of a magnetic field (for instance [146]).

In the case of the solidification of a magnetically non-isotropic atomic structure, the application of a strong magnetic field (several teslas) results in an orientation of all the grains in the same direction[147]. This is used in practice to produce anisotropic materials with specific electric properties along one direction like superconducting rods.

6.3 Magnetic dependence of thermo-physical properties

More generally, a magnetic field should affect all thermo-physical coefficients as an independent generalized force applied to a thermodynamic system (here the material studied). In reference [148], Youdelis *et al.* used condensed matter theories and stated that solute diffusivity and

liquidus and solidus temperatures could be dependent on the magnetic field. The same authors also performed some experiments, that seem to support their theoretical conclusions. Recently, new experiments were reported [149] were effects predicted and reported experimentally by Youdelis *et al.* were invalidated (see [149]). In the reference [149], a $3.5T$ magnetic field is reported to have no effect on liquidus temperature of AlCu or AlSi alloys, nor on their eutectic temperature, whereas Youdelis *et al.* found an effect. Regarding solute diffusivities, our opinion is that the discrepancy concerning the experimental data can be explained by disturbing convective effects: the measurements assume that there is no convection (see Garandet *et al.* [150] for the measurement of solute diffusivities) while in reality convective effects can play a role. In the case when a magnetic field is applied, it may reduce significantly the convective contribution to the measurement. So, some experiments reporting effects of a magnetic field on thermophysical properties may be just related to the damping Lorentz force of convection. Nevertheless, the real effect of the magnetic field on thermophysical properties can not be denied *a priori* and further careful experimental studies are needed. For instance, the analysis of the magnetic force on the boundary of a material shows that the surface tension is modified in the presence of a strong magnetic field [142, 151]. Again, the effect is quite weak and should be sensitive only for magnetic fields larger than several teslas. In the case of a Bridgman configuration with a free surface, this effect may add to the classical Marangoni convection. In any case, the striking point is the knowledge of the limit of the damping effect of the magnetic field (see for instance the measurement of diffusivities [152]). It may be interesting to apply a very high magnetic field, provided the thermophysical properties are unchanged.

7 Concluding remarks

In most applications of Bridgman growth under magnetic fields, the objective is to act on solute segregation through a modification of the convective flows in the melt. Our purpose in this contribution was to review the obtained modelling and experimental results to outline the various physical mechanisms involved and to assess their relevance to a given process using rule of thumb scaling laws. Since it was obviously not possible to get into the details of each problem, the interested reader is often referred to the original publications for a more comprehensive discussion.

Nevertheless, some trends were clearly identified in the course of this work. For instance, it was seen that relatively modest magnetic fields (say in the $0.01T$ to $0.1T$ range) were very efficient in damping hydrodynamic fluctuations and the induced solute striations, almost irrespectively of the magnetic lines orientation. The damping effect can be attributed to Joule dissipation affecting both the basic flow and the possible distubances.

The efforts aiming at the obtaining of diffusion controlled solute transport conditions using static magnetic fields in the tesla range were less conclusive. A significant decrease of the convection level was indeed achieved, depending highly on the magnetic field orientation and more generally on the global symmetry of the configuration. Nevertheless, the efficiency of the field in terms of mass transport was seen to be reduced in the vicinity of the growth interface due to the local interaction of the hydrodynamic and the solute boundary layers. Besides, a lower

fluid velocity may lead to an increase of the radial segregation, meaning that the overall effect of the magnetic field in terms of composition homogeneity is not necessarily positive.

Rotating magnetic fields were seen to be an efficient way to act on both heat and mass transfer in the melt thanks to the high convection velocities driven by the Lorentz force. One can thus reduce the curvature of the solid liquid interface and the radial segregation. However, the flow may become unsteady at excessive rotation frequencies and/or magnetic inductions, meaning that the overall influence of the field on the growth process can again be deleterious.

Another aspect to be considered is that a variety of miscellaneous problems (*e.g.* thermoelectric magnetohydrodynamics or magnetic volume forces) are associated with the presence of a magnetic field. Even though some of these effects are indeed secondary, our review indicates that they should not be *a priori* overlooked. For instance, the interaction of thermoelectric currents along the interface with an imposed magnetic field can have a key impact on fluid flow and mass transfer.

Our overall conclusion would be that, in Bridgman solidification of electrically conducting fluids, the application of a suitable magnetic field is an interesting way to improve the quality of the grown crystals. Nevertheless, for the technique to be really useful, all the aspects of the transport problem should be first carefully analyzed.

Acknowledgements

The present work was carried out partly in the frame of the GRAMME agreement between the Centre National d'Études Spatiales and the Commissariat à l'Énergie Atomique and partly under the grant 97/CNES/071/6881 from the Centre National d'Études Spatiales. It is a pleasure to thank Ph. Marty for perusing and improving the manuscript.

References

[1] W.A. Gault, E.M. Monberg, and J.E. Clemans. A novel application of the vertical gradient freeze method to the growth of high-quality III-V crystals. *J. Crystal Growth*, **74**(3):491–506, 1986.

[2] E.M. Monberg, H. Brown, and C.E. Bonner. The dynamic gradient freeze growth of InP. *J. Crystal Growth*, **94**(1):109–114, 1989.

[3] P. Capper. Bridgman growth of $Cd_xHg_{1-x}Te$ – a review. *Prog. Crystal Growth Charact.*, **19**:259–293, 1989.

[4] P. Cheuvart, U. El-Hanani, D. Schneider, and R. Triboulet. CdTe and CdZnTe crystal-growth by horizontal Bridgman technique. *J. Crystal Growth*, **101**(1–4):270–274, 1990.

[5] F. Allegretti, B. Borgia, R. Riva, F. De Notaristefani, and S. Pizzini. Growth of BGO single-crystals using a directional solidification technique. *J. Crystal Growth*, **94**(2):373–380, 1989.

[6] S. Pinol, J. Fontcuberta, and C. Miravitlles. High-temperature superconductor composites by a modified Bridgman method. *J. Crystal Growth*, **100**(1-2):286–292, 1990.

[7] T. Duffar, J.M. Gourbil, P. Boiton, P. Dusserre, and N. Eustathopoulos. Full encapsulation by molten salts during the Bridgman growth process. *J. Crystal Growth*, **179**:356–362, 1997.

[8] H.P. Utech and M.C. Flemings. Elimination of solute banding in indium antimonide crystals by growth in a magnetic field. *Journal of Applied Physics*, **37**(5):2021–2024, 1966.

[9] D.H. Matthiesen, M.J. Wargo, S. Motakef, D.J. Carlson, J.S. Nakos and A.F. Witt. Dopant segregation during vertical Bridgman-Stockbarger growth with melt stabilization by strong axial magnetic fields. *J. Crystal Growth*, **85**:557–560, 1987.

[10] T. Alboussière, A.C. Neubrand, J.P. Garandet, and R. Moreau. Segregation during horizontal Bridgman growth under an axial magnetic field. *J. Crystal Growth*, **181**:133–144, 1997.

[11] P. Dold and K.W. Benz. Modification of fluid flow and heat transport in vertical Bridgman configurations by rotating magnetic fields. *Cryst. Res. Techno.*, **32**(1):51–60, 1997.

[12] J Friedrich, C. Kupfer, B. Fischer, and G. Müller. Influence of rotating magnetic fields on heat and species transport in crystal growth by the vertical gradient freeze method. In *Fluid Mechanics and its Applications*. Kluwer Ed., The Netherlands, 1998.

[13] J.S. Walker and M.G. Williams. Effects of the crystal nonzero electrical-conductivity on the rotationally driven melt motion during Czochralski silicon growth with a uniform, transverse magnetic-field. *J. Crystal Growth*, **132**(1-2):31–42, 1993.

[14] Eds. R. Ueda and J.B. Mullin. *Crystal Growth and Characterization*. North Holland, 1975.

[15] F. Rosenberger. *Fundamentals of Crystal Growth I. Macroscopic Equilibrium and Transport Concepts*. Springer Verlag, 1979.

[16] Ed. H.U. Walter. *Fluid Sciences and Materials Science in Space*. Springer Verlag, 1987.

[17] G. Müller. *Crystals, Growth, Properties and Applications*, volume **12** . Springer Verlag, 1988.

[18] J.P. Garandet, J.J. Favier and D. Camel. *Segregation phenomena in crystal growth from the melt. chapter 12 of "Handbook of crystal growth", vol. 2.* Edited by D.T.J. Hurle. North Holland, 1994.

[19] P. Rudolph, T. Boeck, and P. Schmidt. Thermodiffusion and morphological stability in convectionless crystal-growth systems from melts and melt-solutions. *Cryst. Res. Technol.* **31**(2):221–229, 1996.

[20] S. Van Vaerenbergh, S.R. Coriell, G.B. *Mc* Fadden, B.T. Murray, and J.C. Legros. Modification of morphological stability by soret diffusion. *J. Crystal Growth*, **147**(1–2):207–214, 1995.

[21] K. Kakimoto, M. Eguchi, H. Watanabe, and T. Hibiya. In-situ observation of impurity diffusion boundary-layer in silicon czochralski growth. *J. Crystal Growth*, **99**(1–4):665–669, 1990.

[22] R.M. Sharp and A. Hellawell. The microscopy and composition of quenched solid-liquid interfaces. *J. Crystal Growth*, **5**:155–161, 1969.

[23] B. Billia. *Recherches sur la morphologie du front de solidification lors de la croissance unidirectionnelle d'alliages binaires.* PhD dissertation, Université Aix-Marseille, 1982.

[24] J.I.D Alexander, J. Wazzani, and F. Rosenberger. Analysis of the low gravity tolerance of Bridgman-Stockbarger crystal growth. I. Steady and impulsive accelrations. *J. Crystal Growth*, **97**:285–302, 1989.

[25] C.J. Chang and R.A. Brown. Radial segregation induced by natural convection and melt/solid interface shape in vertical Bridgman growth. *J. Crystal Growth*, **63**:343–364, 1983.

[26] S. Kaddeche, H. Ben Hadid, and D. Henry. Macrosegregation and convection in the horizontal Bridgman configuration. I. Dilute alloys. *J. Crystal Growth*, **135**:341–353, 1994.

[27] T. Jung and G. Müller. Amplitudes of doping striations: comparison of numerical calculations and analytical approaches. *J. Crystal Growth*, **171**:373–379, 1997.

[28] J.A. Burton, R.C. Prim and W.P. Slichter. The distribution of solute in crystals grown from the melt. Part I. Theoretical. *The Journal of Chemical Physics*, **21**(11):1987–1991, 1953.

[29] C. Wagner. Theoretical analysis of diffusion of solute during the solidification of alloys. *J. Metals*, **6**:154–160, 1954.

[30] L.O. Wilson. On interpreting a quantity in the Burton, Prim and Schlichter equation as a diffusion boundary layer thickness. *J. Crystal Growth*, **44**:247–250, 1978.

[31] C.C. Lin and L.A. Segel. *Mathematics Applied to Deterministic problems in the Material Sciences.* Macmillan, 1974.

[32] A. Bejan. *Convection Heat Transfer.* Wiley and sons, 1984.

[33] J.P. Garandet, T. Duffar, and J.J. Favier. On the scaling analysis of the solute boundary layer in idealized growth configurations. *J. Crystal Growth*, **106**:437–444, 1990.

[34] J.P. Garandet, T. Duffar, and J.J. Favier. Vertical gradient freeze growth of ternary GaAs-InSb crystals. *J. Crystal Growth*, **106**(2–3):426–436, 1990.

[35] S. Kaddeche, J.P. Garandet, C. Barat, H. Ben Hadid, and D. Henry. Interface curvature and convection related macrosegregation in the vertical Bridgman configuration. *J. Crystal Growth*, **158**(1–2):144–152, 1996.

[36] J.P. Garandet, A. Rouzaud, T. Duffar, and D. Camel. Comparison between order of magnitude and numerical estimates of the solute boundary layer in an idealized horizontal Bridgman configuration. *J. Crystal Growth*, **113**:587–592, 1991.

[37] W.A. Tiller, K.A. Jackson, J.W. Rutter, and B. Chalmers. The redistribution of solute atoms during the solidification of metals. *Acta Met.*, **1**:428–437, 1953.

[38] E. Scheil. Bemerkungen zur Schichtkristallbildung. *Z. Metall.*, **34**:70–72, 1942.

[39] W.W. Mullins and R.F. Sekerka. Stability of a planar interface during solidification of a dilute binary alloy. *J. Appl. Phys.*, **35**:444–451, 1964.

[40] B. Caroli, C. Caroli, and B. Roulet. On the emergence of one-dimensional front instabilities in directional solidification and fusion of binary-mixtures. *J. Physique*, **43**:1767–1780, 1982.

[41] J.J. Favier and A. Rouzaud. Morphological stability of the solidification interface under convective conditions. *J. Crystal Growth*, **64**:367–379, 1983.

[42] A.F. Witt, H.C. Gatos, M. Lichtensteiger, M.C. Lavine, and C.J. Hermann. Crystal growth and steady state segregation under zero gravity: InSb. *J. Electrochem. Soc.*, **122**:276–283, 1975.

[43] A.F. Witt, H.C. Gatos, M. Lichtensteiger, and C.J. Hermann. Crystal growth and segregation under zero gravity: Ge. *J. Electrochem. Soc.*, **125**:1832–1840, 1978.

[44] J.J. Favier, J. Berthier, P. Arragon, Y. Malmejac, V.T. Khryapov, and I.V. Barmin. Solid liquid interface stability in normal and microgravity conditions – the ELMA 01 experiments. *Acta Astronautica*, **9**(4):255–259, 1982.

[45] S. Motakef. Thermoelastic study of GaAs in vertical gradient freeze configuration – Limits to the optimum growth rate and approaches to its augmentation. *J. Crystal Growth*, **98**(4):711–720, 1989.

[46] R.S. Feigelson and R.K. Route. Vertical Bridgman growth of $CdGeAs_2$ with control of interface shape and orientation. *J. Crystal Growth*, **49**:261–273, 1980.

[47] C.E. Huang, D. Elwell, and R.S. Feigelson. Influence of thermal conductivity on interface shape during Bridgman growth. *J. Crystal Growth*, **64**(3):441–447, 1983.

[48] T. Jasinski, A.F. Witt, and W.M. Rohsenow. Heat transfer analysis of the Bridgman-Stockbarger configuration for crystal growth. II. Analytical treatment of radial temperature variations. *J. Crystal Growth*, **67**(2):173–184, 1984.

[49] S.R. Coriell and R.F. Sekerka. Lateral solute segregation during unidirectional solidification of a binary alloy with a curved solid-liquid interface. *J. Crystal Growth*, **46**:479–482, 1979.

[50] S.R. Coriell, R.F. Boisvert, R.G. Rehm, and R.F. Sekerka. Lateral solute segregation during unidirectional solidification of a binary alloy with a curved solid-liquid interface. II. Large departures from planarity. *J. Crystal Growth*, **54**(2):167–175, 1981.

[51] R.J. Naumann. Modelling flows and solute redistribution resulting from small transverse accelerations in Bridgman growth. *J. Crystal Growth*, **142**(1–2):253–267, 1994.

[52] J.P. Garandet. On the problem of radial segregation in an idealized horizontal Bridgman configuration – Scaling and numerical approaches. *J. Crystal Growth*, **114**(4):593–602, 1991.

[53] J.P. Garandet. Convection related radial segregation in an idealized horizontal Bridgman configuration – The quasi diffusive regime limit. *J. Crystal Growth*, **125**(1–2):112–120, 1992.

[54] R.J. Naumann and C. Baugher. Analytical estimates of radial segregation in Bridgman growth from low-level steady and periodic accelerations. *J. Crystal Growth*, **121**(4):751–768, 1992.

[55] P.M. Adornato and R.A. Brown. Convection and segregation in directional solidification of dilute and non-dilute binary-alloys – Effects of ampoule and furnace design. *J. Crystal Growth*, **80**(1):155–190, 1987.

[56] S. Motakef. Interference of buoyancy-induced convection with segregation during directional solidification – scaling laws. *J. Crystal Growth*, **102**(1–2):197–213, 1990.

[57] C. Wang. ScD thesis, Massachussetts Institute of Technology, 1984.

[58] A. Rouzaud, D. Camel, and J.J. Favier. A comparative study of thermal and thermosolutal convective effects in vertical Bridgman crystal growth. *J. Crystal Growth*, **73**(1):149–166, 1985.

[59] T. Nishinaga, T. Kazuno, T. Tanbo, J. Koide, K. Pak, T. Nakamura, and Y. Yasuda. Behavior of macrosteps and grooves during LPe growth as observed by photoluminescence images. *J. Crystal Growth*, **65**(1–3):607–610, 1983.

[60] A.N. Danilewsky and K.W. Benz. InP growth from In solutions under reduced gravity. *J. Crystal Growth*, **97**(3–4):571–577, 1989.

[61] D.T.J. Hurle, E. Jakeman, and E.R. Pike. Striated solute distributions produced by temperature oscillations during crystal growth from the melt. *J. Crystal Growth*, **3, 4**:633–640, 1968.

[62] D. Thévenard, A. Rouzaud, J. Coméra, and J.J. Favier. Influence of convective thermal oscillations on a solidification interface in Bridgman growth. *J. Crystal Growth*, **108**(3–4):572–582, 1991.

[63] J.P. Garandet. Microsegregation in crystal growth from the melt – An analytical approach. *J. Crystal Growth*, **131**(3–4):431–438, 1993.

[64] J.P. Garandet, S. Corre, S. Gavoille, J.J. Favier, and J.I.D. Alexander. On the effect of gravity perturbations on composition profiles during Bridgman crystal growth in space. *J. Crystal Growth*, **165**(4):471–481, 1996.

[65] S. Corre. *Phénomènes instationnaires et ségrégation solutale en solidification Bridgman.* PhD dissertation, Institut National Polytechnique de Grenoble, Grenoble CENG/DEM/LRBS, 1997.

[66] F. Haddad and D. Henry. *Ecole Centrale de Lyon internal report, to be published in J. Crystal Growth*, : , 1998.

[67] A.F. Witt, M. Lichtensteiger, and H.C. Gatos. Experimental approach to the quantitative determination of dopant segregation during crystal growth on a microscale: Ga doped Ge. *J. Electrochem. Soc.*, **120**:1119–1123, 1972.

[68] F. Debray, L. Davoust, Y. Fautrelle, and J. Étay. Measurement and electrochemical analysis of solute convection at the interface of two liquids with and without a magnetic field. *Int. J. Heat Mass Transf.*, **40**:1985–1989, 1997.

[69] J.E. Hart. On sideways diffusive instability. *J. Fluid Mech*, **49**:279–288, 1971.

[70] R.K. Crouch, A.L. Fripp, W.J. Debnam, I.O. Clark, P.G. Barber, and F.M. Carlson. Experimental investigation of the effects of gravity on thermosolutal convection and composition homogeneity in Bridgman grown, compound semiconductors. In *Proc. 35th Congress International Astronautical Federation*, Lausanne, Switzerland, 1984.

[71] H. Jamgotchian, B. Billia, and L. Capella. Thermosolutal convection induced morphologies of the solid liquid interface during upward solidification of Pb-30 *w*%-Tl alloys. *J. Crystal Growth*, **82**(3):342–350, 1987.

[72] A. Mueller and M. Wihelm. *Z. Naturforsch.*, **19a**:254–, 1964.

[73] R. Moreau. *Magnetohydrodynamics.* Kluwer Acad. Publ., 1990.

[74] A.N. Danilewsky, P. Dold and K.W. Benz. The influence of axial magnetic fields on the growth of III-V semiconductors from metallic solutions. *J. Crystal Growth*, **121**:305–314, 1992.

[75] P. Becla, J.C. Han, and S. Motakef. Application of strong vertical magnetic fields to growth of II–VI pseudo-binary alloys: HgMnTe. *J. Crystal Growth*, **121**:394–398, 1992.

[76] S. Sen, R.A. Lefever, and W.R. Wilcox. Influence of magnetic field on vertical Bridgman-Stockbarger growth of $In_xGa_{1-x}Sb$. *J. Crystal Growth*, **43**:526–530, 1978.

[77] K.M. Kim. Suppression of thermal convection by transverse magnetic field. *J. Electrochem. Soc.*, **129**(2):427–429, 1982.

[78] S. Chandrasekhar. *Hydrodynamic and Hydromagnetic stability*. Oxford University Press, 1961.

[79] P. Dold and K.W. Benz. Convective temperature fluctuations in liquid gallium in dependence on static and rotating magnetic fields. *Cryst. Res. Technol.*, **30**(8):1135–1145, 1995.

[80] D.T.J. Hurle, E. Jakeman and C.P. Johnson. Convective temperature oscillations in molten gallium. *J. Fluid Mech.*, **64**(3):565–576, 1974.

[81] R.V. Birikh. Thermocapillary convection in a horizontal layer of liquid. *Zhurnal Prikladnoi Mekhaniki i Teckhnicheskoi Fisiki*, **3**:69–72, 1966.

[82] J.E. Hart. Stability of thin non-rotating Hadley circulations. *J. Atmos. Sci.*, **29**:687–697, 1972.

[83] A.E. Gill. A theory of thermal oscillations in liquid metals. *J. Fluid Mech.*, **64**(3):577–588, 1974.

[84] J.E. Hart. A note on the stability of low-Prandtl number Hadley circulations. *J. Fluid Mech.*, **132**:271–281, 1983.

[85] J.E. Hart. Low Prandtl number convection between differentially heated end walls. *Int. J. Heat Mass Transfer*, **26**(7):1069–1074, 1983.

[86] J.M. Pratte and J.E. Hart. Endwall driven, low Prandtl number convection in a shallow rectangular cavity. *J. Crystal Growth*, **102**:54–68, 1990.

[87] M. Afrid and A. Zebib. Oscillatory three-dimensional convection in rectangular cavities and enclosures. *Phys. Fluids A*, **2**(8):1318–1327, 1990.

[88] M.J. Crochet, F.T. Geyling, and J.J. Van Schaftingen. Numerical simulation of the horizontal Bridgman growth. Part I: two-dimensional flow. *Int. J. Numer. methods fluids*, **7**:29–47, 1987.

[89] S. Dupont, J.M. Marchal, M.J. Crochet, and F.T. Geyling. Numerical simulation of the horizontal Bridgman growth. Part II: three-dimensional flow. *Int. J. Numer. methods fluids*, **7**:49–67, 1987.

[90] H.P. Kuo and S.A. Korpela. Stability and finite-amplitude natural convection in a shallow cavity with insulated top and bottom and heated from a side. *Phys. Fluids*, **31**(1):33–42, 1988.

[91] L. Davoust. *Convection naturelle MHD dans une cavité horizontale élancée*. PhD dissertation, Institut National Polytechnique de Grenoble, Madylam, Grenoble, 1996.

[92] R.V. Birikh, G.Z. Gershuni, E.M. Zhukovitskii, and R.N. Rudakov. Stability of convective flow of a conducting fluid in a magnetic field. *Magnitnaya Gidrodinamika*, 1:30–36, 1978.

[93] H. Ben Hadid, D. Henry, and S. Kaddeche. Numerical study of convection in the horizontal Bridgman configuration under the action of a constant magnetic field. Part 1. Two-dimensional flow. *J. Fluid Mech.*, **333**:23–56, 1997.

[94] L. Davoust, R. Moreau, R. Bolcato, T. Alboussière, A.C. Neubrand, and J.P. Garandet. Influence of a vertical magnetic field in on convection in the horizontal Bridgman crystal growth configuration. In *2nd Int. Conf. on Energy Transfer in Magnetohydrodynamic flows*, PAMIR, Aussois, France, Sept 1994.

[95] P.A. Davidson. Magnetic damping of jets and vortices. *J. Fluid Mech.*, **299**:153–186, 1995.

[96] D.H. Kim, P.M. Adornato, and R.A. Brown. Effect of vertical magnetic field on convection and segregation in vertical Bridgman crystal growth. *J. Crystal Growth*, **89**:339–356, 1988.

[97] D.A. Watring and S.L. Lehoczky. Magneto-hydrodynamic damping of convection during vertical Bridgman-Stockbarger growth of HgCdTe. *J. Crystal Growth*, **167**(3–4):478–487, 1996.

[98] D.A. Watring. The effects of vertical magnetic fields on segregation in HgCdTe. *Materials Science Forum*, **215**:363–368, 1996.

[99] D.H. Matthiesen, M.J. Wargo, and A.F. Witt. Ch. 4a. In G.A. Hazelrigg and J.M. Reynolds, editors, *Opportunities for Academic Research in a low-gravity environment*, Progress in Astro- and Aero., AIAA, pages 124–144, New York, Sept 1986.

[100] G.M. Oreper and J. Szekely. The effect of a magnetic field on transport phenomena in a Bridgman-Stockbarger crystal growth. *J. Crystal Growth*, **67**:405–419, 1984.

[101] S. Motakef. Magnetic field elimination of convective interference with segregation during vertical-Bridgman growth of doped semiconductors. *J. Crystal Growth*, **104**(4):833–850, 1990.

[102] V. Uspenskii and J.J. Favier. High frequency vibration and natural convection in Bridgman-scheme crystal growth. *Int. J. Heat Mass Transfer*, **37**(4):691–698, 1994.

[103] M. Yao, A. Chait, A.L. Fripp, and W.J. Debnam. Magnetically damped convection and segregation in Bridgman growth of PbSnTe. *J. Crystal Growth*, **173**:467–480, 1997.

[104] A.C. Neubrand, T. Alboussière, and J.P. Garandet. Magnetic field and segregation during bridgman growth. 9th European Symposium "Gravity Dependant Phenomena in Physical Sciences, Berlin, Germany, May 1995.

[105] A.C. Neubrand. *Convection naturelle et ségrégation en solidification Bridgman sous champ magnétique.* PhD dissertation, Institut National Polytechnique de Grenoble, Grenoble CENG/DEM/SES, 1995.

[106] L.N. Hjellming and J.S. Walker. Melt motion in a Czochralski crystal puller with an axial magnetic field: isothermal motion. *J. Fluid Mech.*, **164**:237–273, 1986.

[107] T. Alboussière, J.P. Garandet, and R. Moreau. Asymptotic analysis and symmetry in MHD convection. *Phys. Fluids*, **8**(8):2215–2226, 1996.

[108] J.P. Garandet, T. Alboussière, and R. Moreau. Buoyancy driven convection in a rectangular enclosure with a transverse magnetic field. *Int. J. Heat and Mass Transfer*, **35**(4):741–748, 1992.

[109] G.Z. Gershuni and E.M. Zhukovitskii. Stationary convective motion of an electrically conducting fluid between parallel planes in a magnetic field. *Zh. Éksp. Teor. Fiz.*, **34**(3):670–674, 1958.

[110] G.M. Oreper and J. Szekely. The effect of an externally imposed magnetic field on buoyancy driven flow in a rectangular cavity. *J. Crystal Growth*, **64**:505–515, 1983.

[111] S. Alchaar, P. Vasseur, and E. Bilgen. Natural convection heat transfer in a rectangular enclosure with a transverse magnetic field. *J. Heat Transfer*, **117**:668–673, 1995.

[112] T. Alboussière, J.P. Garandet, and R. Moreau. Buoyancy-driven convection with a uniform magnetic field. Part I. Asymptotic analysis. *J. Fluid Mech.*, **53** :545–563, 1993.

[113] A.V. Boyarevich and L.A. Gorbunov. Effect of magnetic fields of different orientation on thermogravitational convection in an electrically conducting fluid with a horizontal heat flow. *Magnetohydrodynamics*, **2**:148–154, 1988.

[114] K. Okada and H. Ozoe. Experimental heat transfer rates of natural convection of molten gallium suppressed under an external magnetic field in either the x, y, or z direction. *J. Heat Transfer*, **114**:107–114, 1992.

[115] L. Davoust, R. Moreau, M.D. Cowley, P.A. Tanguy, and F. Bertrand. Numerical and analytical modelling of the MHD buoyancy-driven flow in a Bridgman crystal growth configuration. *J. Crystal Growth*, **180**:422–432, 1997.

[116] H. Ben-Hadid and D. Henry. Numerical simulation of convective 3-dimensional flows in a horizontal cylinder under the action of a constant magnetic field. *J. Crystal Growth*, **166**(1–4):436–445, 1996.

[117] H. Ben Hadid and D. Henry. Numerical study of convection in the horizontal Bridgman configuration under the action of a constant magnetic field. Part 2. Three-dimensional flow. *J. Fluid Mech.*, **333**:57–83, 1997.

[118] S. Kaddeche, H. Ben Hadid, and D. Henry. Macrosegregation and convection in the horizontal Bridgman configuration. I. Dilute alloys. *J. Crystal Growth*, **135**:341–353, 1994.

[119] N. Ma and J.S. Walker. Magnetic damping of buoyant convection during semiconductor crystal growth with g-jitters. *J. of Thermophysics and Heat Transfer*, **11**(2):212–215, 1997.

[120] N. Ma and J.S. Walker. Dopant transport during semiconductor crystal growth with magnetically damped buoyant convection. *J. Crystal Growth*, **172**:124–135, 1997.

[121] T. Alboussière. *Magnétohydrodynamique et ségrégation solutale en croissance Bridgman horizontale.* PhD dissertation, Institut National Polytechnique de Grenoble, Grenoble CENG/DEM/SES, 1994.

[122] M. Cowley. On the temperature distribution due to convection in the horizontal Bridgman crystal growth configuration with vertical magnetic field. *Magnetohydrodynamics*, **31**(3):236–244, 1995.

[123] N. Ma, K.O. Homan, and J.S. Walker. Magnetic damping of buoyant convection during semiconductor crystal growth in microgravity. Steady transverse residual acceleration. *Phys. Fluids*, **9**(9):2789–2797, 1997.

[124] N. Ma and J.S. Walker. Magnetic damping of buoyant convection during semiconductor crystal growth in microgravity. Continuous random g-jitters. *Phys. Fluids*, **8**(4):944–953, 1996.

[125] P.A. Davidson. Swirling flow in an axisymmetric cavity of arbitrary profile, driven by a rotating magnetic field. *J. Fluid Mech.*, **245**:669–699, 1992.

[126] P.A. Davidson, D.J. Short, and D. Kinnear. The role of Ekman pumping in confined electromagnetically-driven flows. *Eur. J. Mech. B*, **14**(6):795–821, 1995.

[127] L. Martin-Witkowski. *Écoulements engendrés par un champ magnétique tournant en geéométrie cylindrique.* PhD dissertation, Institut National Polytechnique de Grenoble, LEGI, Grenoble, 1997.

[128] Ph. Marty, L. Martin Witkowski, P. Trombetta, T. Tomasino, and J.P. Garandet. On the stability of rotating MHD flows. In *Fluid Mechanics and its Applications*. Kluwer Ed., The Netherlands, 1998.

[129] F.U. Bruckner and K. Schwerdtfeger. Single crystal growth with the czochralskii method involving rotational electromagnetic stirring of the melt. *J Crystal Growth*, **139**(3–4):351–356, 1994.

[130] Y.M. Gelfgat and L.A. Gorbunov. Effects of alternating magnetic fields on melt hydrodynamics in a cylindrical vessel with free surface. *Magnetohydrodynamics*, **30**:237–247, 1994.

[131] A.T. Richardson. On the stability of a magnetically driven rotating fluid flow. *J. Fluid Mech.*, **63**:593–605, 1974.

[132] T. Kaiser and K.W. Benz. Taylor vortex instabilities induced by a rotating magnetic field: A numerical approach. *Physics of Fluids*, **10**(5):1104–1110, 1998.

[133] P. Dold and K.W. Benz. Convective temperature fluctuations in liquid gallium in dependence on static and rotating magnetic fields. *Cryst. Res. Technol.*, **30**:1135–1145, 1995.

[134] M.P. Volz and K. Mazuruk. Flow transitions in a rotating magnetic field. *Experiments in fluids*, **20**(6):454–459, 1996.

[135] P. Marty, J.P. Trombetta, and J.P. Garandet. Contrôle de la stabilité d'un écoulement thermoconvectif par un champ magnétique tournant. *C. R. Acad. Sci. Paris II-b*, **326**:185–190, 1998.

[136] J.A. Shercliff. Thermoelectric magnetohydrodynamics. *J. Fluid Mech.*, **91**:231–251, 1979.

[137] Y. Gelfgat and L.A. Gorbunov. An additional source of forced convection in semiconductor melts during single crystal growth in magnetic fields. *Sov. Phys. Dokl.*, **34**:470–473, 1989.

[138] Y.Y. Khine and J.S. Walker. Thermoelectric magnetohydrodynamic effects during Bridgman growth with a uniform axial magnetic field. *J. Crystal Growth*, **183**:150–158, 1998.

[139] Y.Y. Khine and J.S. Walker. Thermoelectric magnetohydrodynamic effects during Bridgman semiconductor crystal growth with a uniform axial magnetic field: large Hartmann number asymptotic solution. In *Fluid Mechanics and its Applications*. Kluwer Ed., The Netherlands, 1998.

[140] R. Moreau, O. Laskar, M. Tanaka, and D. Camel. Thermoelectric magnetohydrodynamic effects on solidification of metallic alloys in the dendritic regime. *Materials Sci. Eng. A*, **173**:93–100, 1993.

[141] A. Cröll, F.R. Szofran, P. Dold, K.W. Benz, and S.L. Lehoczky. Floating zone growth of silicon in magnetic fields. II. Strong axial fields. *J. Crystal Growth*, **183**:554–563, 1998.

[142] W.F. Brown. Electric and magnetic forces: a direct calculation. I. *Am. J. Phys.*, **19**:290–304, 1951.

[143] E. Beaugnon and R. Tournier. Levitation of water and organic substances in high static magnetic fields. *J. Phys. III France*, **1**:1423–1428, 1991.

[144] D. Braithwaite, E. Beaugnon, and R. Tournier. Magnetically controlled convection in a paramagnetic fluid. *Nature*, **354**, 1991.

[145] N.W. Price, R.N. Andrews, C.H. Su, S.L. Lehoczky, and F.R. Szofran. The effect of a transverse magnetic field on the microstructure of directionally solidified CdTe. *J. Crystal Growth*, **137**:201–207, 1994.

[146] Y. Aoki, S. Hayashi, and H. Komatsu. The effect of magnetic field on crystallization of γ-phase alloy in the CuZn system. *J. Crystal Growth*, **108**:121–128, 1991.

[147] E. Beaugnon. *Les champs magnétiques statiques dans la synthèse des matériaux ; étude expérimentale de systèmes modèles.* PhD dissertation, Institut National Polytechnique de Grenoble, Grenoble CNRS/CRTBT, 1992.

[148] W.V. Youdelis. D.R. Colton, and J. Cahoon. On the theory of diffusion in a magnetic field. *Can. J. of Phys.*, **42**:2217–2237, 1964.

[149] Y. Aoki, S. Hayashi, and H. Komatsu. Liquidus and eutectic temperature measurements of Al-rich alloys containing Cu and Si in a magnetic field of 3.5 T. *J. Crystal Growth*, **123**:313–316, 1992.

[150] J.P. Garandet, C. Barat, and T. Duffar. On the effect of natural convection in mass transport measurements in dilute liquid alloys. *Int. J. Heat Mass Transfer*, **38**:2169–2174, 1995.

[151] L. Liggieri, A. Sanfeld, and A. Steinchen. Effects of magnetic and electric fields on surface tension of liquids. *Physica A*, **206**:299–331, 1994.

[152] T. Alboussière, J.P. Garandet, P. Lehmann, and R. Moreau. Measurement of solute diffusivity in electrically conducting liquids. In *Fluid Mechanics and its Applications.* Kluwer Ed., The Netherlands, 1998.

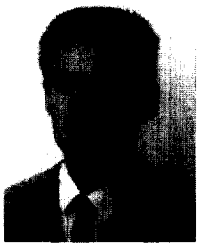

Dr Jean-Paul Garandet
Centre d'Études Nucléaires de Grenoble
17 rue des Martyrs
38054 Grenoble Cedex
France

J.P. Garandet graduated from the École Nationale Supérieure des Télécommunications de Paris in 1983. He holds a doctorate in Material Sciences from the Institut National Polytechnique de Grenoble. He has been working in the solidification lab of the CEA-Grenoble since 1989.

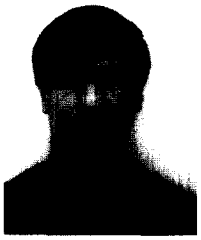

Dr Thierry Alboussière
Department of Engineering
University of Cambridge
Trumpington Street
Cambridge CB2 1PZ
UK

T. Alboussière graduated from the École Nationale Supérieure d'Hydraulique et de Mécanique de Grenoble in 1990 and got a PhD in mechanics from the Institut National Polytechnique de Grenoble. He is a lecturer in the Cambridge Engineering Department since 1996.